

Interactive comment on “Effects of 238 variability and physical transport on water column 234Th downward fluxes in the coastal upwelling system off Peru” by Ruifang Xie et al.

Anonymous Referee #1

Received and published: 7 April 2020

Xie et al. present new data of 234Th export fluxes from the coastal upwelling system off Peru, associated with an oxygen minimum zone (OMZ). The aim of this research is to investigate the effects of 238U variability and physical processes on the 234Th fluxes. The authors found a poor correlation between measured (by isotopic dilution) and calculated (from salinity) 238U activities. Even though only small variations were observed between measured and calculated 238U activities, this difference leads to significant underestimation of 234Th fluxes. 238U activities are usually not measured, as this represents additional work and the linear relationship with salinity is generally assumed. However, the current study clearly shows the need for measuring 238U activities in non-open ocean systems. The impact of physical processes, such as advection and diffusion, was evaluated by using ADCP, current velocities, satellite wind stress and in situ microstructure measurements. Unlike horizontal diffusion and advection, vertical diffusion and advection were found to significantly modify the 234Th export fluxes at shelf stations. Again, most studies neglect the impact of physics on 234Th fluxes and rare are those considering vertical/horizontal advection and diffusion effects on 234Th fluxes. Finally, the authors investigated the 234Th residence time and found a large temporal variation across the Peruvian upwelling zone, warning future studies to take into account these temporal changes while evaluating carbon export efficiencies. Overall, the manuscript is well written and represents an important effort. In most studies the influence of the 238U variability and physical processes are assumed to be negligible. The findings of this study are therefore highly valuable for the community. With some reorganisation and some more details on the calculations, this manuscript will be a good fit for publication in Biogeosciences.

We thank the reviewer for his/her constructive comments. We’ve listed our point-by-point response in bold below.

1. Specific comments.

1-Results section. Details are missing to really understand the choices made in the Discussion. I propose to add a “Results” section that would moreover make the discussion clearer for the reader. This new section could present: 1) Total 234Th and 238U activities: basically what is written between the beginning of Section 3 and before the beginning of Section 3.1. 2) Export fluxes of 234Th: - Please give more details on the relevance of estimating fluxes at different horizon depths. First, clearly mention in the Methods that you calculate the export fluxes at 100m and below the mixed layer (ML). Then, in this new Results section, you could explain why

you calculate the fluxes at 2 different depths. Why is it relevant to discuss fluxes at 100m or at the base of the ML for the purpose of this work? Also, explain why you estimate the fluxes “below” the ML and not simply at its base? - Steady state versus non-steady state (it should not be part of the sub-section dedicated to “dynamic advective and diffusive ²³⁴Th fluxes”).

Response: We have now added a new Results section to the manuscript that include details on the ²³⁴Th and ²³⁸U profiles, export of ²³⁴Th fluxes at 100 m and base of the ML (and why we used these two different depths), and comparison of the steady state versus non-steady state models. Please refer to the manuscript for more details.

Due to sampling logistics, we did not sample at the base of the ML, but 5-20 m below the ML. This depth corresponded closely to the EZ depth used in Black et al. (2018) in the same study area. For the purpose of comparison with earlier studies which reported ²³⁴Th fluxes at 100 m, we also calculated ²³⁴Th fluxes at 100 m in this study.

2-More details on the physical processes. Methods, section 2.3: For each physical process (horizontal advection, vertical advection, horizontal diffusion and vertical diffusion), please give details on how the ²³⁴Th fluxes due to these processes are calculated. For example, lines 180-182, how do you use the daily wind stress to estimate the upwelling velocity? Lines 180-182 and lines 189-191: In addition to the cited references, please, briefly explain how VmADCP and in situ microstructure profiler measurements work and how you obtain current velocities or diffusivities from them?

Response: We have now expanded the Methods section to include detailed descriptions of how upwelling rates, VmADCP -derived current velocities and microstructure-derived diffusivities were calculated.

Table 1: As not significant processes, you do not present the ²³⁴Th fluxes due to horizontal advection and diffusion. Please, give the values in Table 1 for comparison.

Response: We grouped stations within a 1° by 1° grid and calculated the average ²³⁴Th for the top layer, and large scale (1° apart) horizontal ²³⁴Th gradients were calculated based on this grouping. We then used average alongshore current velocities and eddy diffusivities for the flux estimation due to horizontal advection and diffusion. These estimations are correct to the first order. As these values were rough estimates, we feel that we should not include them in Table 1. We now explained these in more details in the manuscript.

Discussion, section 3.2: Please, explain in more details how you calculate the vertical and horizontal ²³⁴Th gradients. Explanations about the vertical gradient are for example given by

Black et al. (2018) and are useful for the reader. Moreover, lines 326-329, please, clearly say how you determine the horizontal ^{234}Th gradient. What does “larger spatial scale” mean?

Response: We now specified these details on how we calculated the vertical and alongshore ^{234}Th gradients in the Results section (new subsection 2.3.4).

3-Greater ^{238}U activities in suboxic environment. I am very surprised by these results as I would have expected the opposite, i.e., less U in anoxic/suboxic waters. This is very interesting and I did appreciate reading your possible explanations. I however have some questions about them:

- Lines 265-267: If Fe reduction was going on, it would definitely be associated with U removal to the sediment. Is there enough U adsorbed on oxyhydroxides to outpace U removal?
- Could an oxygenation event such as the one described by Rapp et al. (2020) during the 2015 El Niño be responsible of high U concentrations? Assuming a dynamic OMZ and assuming Uranium needs some time to equilibrate, would it be possible to measure high concentrations in low oxygen waters?

Response to both comments: The presence of high content of organic matter in the Peruvian sediments greatly influence U mobility and promote U sorption onto mineral surfaces, such as Fe hydroxides. However, the reviewer is correct that U reduction and removal should occur when sedimentary Fe reduction took place. This was indeed what was observed on the Peruvian shelf by an earlier study (Scholz et al. 2011). We now significantly toned down the discussion on Fe reduction being the main additional U source to the water column, as we cannot accurately quantify the amount of remobilized adsorbed-U vs. U removal.

The same study by Scholz et al. (2011) further showed considerable diffusive U fluxes out of the sediments along the Peru shelf where both Fe reduction and U reduction took place. This remobilization of U was attributed to ENSO-related transient U re-oxidation and recycling. It was suggested that a minute increase in bottom water oxygen concentration was sufficient to shift the U(VI)/U(IV) boundary by a few centimeters and remobilize authigenic U. The coastal El Niño developed preceding to and during our sampling campaign could induce an oxygenation event large enough to remobilized authigenic U along the Peruvian shelf. We now added this discussion to our manuscript.

We would also like to point out that we have significantly modified the discussion on the U-salinity relationship. We now acknowledged that poor U-salinity correlations were also observed in other open ocean basins, and explored possible explanations for this poor correlation in our study area.

- Lines 270-273: Uranium enhancement related to flooding, strong rainfall and landslide would also come with freshwater. Don't you think this would also affect salinity?

Response: This is a fair point. Flooding likely affected both U and salinity in coastal waters. The addition of freshwater and riverine U may draw the datapoints up and down the conservative mixing line (as shown in Owens et al. 2011). However, this was not the case in our study where majority of the U data points fall above the S-U line defined by Owens et al. (2011), indicative of other governing processes other than conservative mixing. We have disregarded the discussion of coastal flooding being one of the main causes of the poor U-salinity correlation.

4-Residence times of ^{234}Th . Lines 371-372: Please, explain how you estimate the residence times.

Response: We now specified in the Methods section the formulation and details on how we calculated the residence times.

2. Line notes.

Line 97, line 104, line 113 and line 676: Keep similar wording all along the text and use "shelf-offshore transect" instead of "shelf-normal" or "shore-normal" transect.

Response: We now used the wording "shelf-offshore transect" instead of the technical term "shore-normal transect".

Line 42: add "e.g." at the beginning of the citation list. There are many more studies.

Response: fixed

Lines 119-120: Please, give the deep ocean average $^{234}\text{Th}/^{238}\text{U}$ ratio in your study.

Response: We now added this average $^{234}\text{Th}/^{238}\text{U}$ ratio in the Results section

Lines 167-168: Please, mention that fluxes are also estimated at 100m. You should also explain the reason of calculating fluxes at both 100m and at 5-20m below the ML for the relevance of this study – as justified for EZ and ML.

Response: We now specified in the Results section why we chose two different depths for the flux calculation.

Line 183: “the depths correspond to 5-20m below the base of the ML”, please mention that this is the reason why you calculate export fluxes at this horizon depth.

Response: fixed

Line 203: would yield a maximum., instead of would a yield maximum..

Response: fixed

Lines 203-206: Maybe to move to the new “Results” section.

Response: fixed

Lines 217-219: Please, provide the number of replicates for the IAPSO standard seawater: “3.24 ± 0.06 ng/g, 1SD, n=?”.

Response: fixed

Lines: 249-254: “The consequence of this notable difference in ^{238}U to ^{234}Th flux according to Eq. (2) is neither linear nor straightforward, because the vertical gradients of both ^{238}U and ^{234}Th strongly affects the impacts of ^{238}U variations on ^{234}Th fluxes. In this study, ^{234}Th fluxes at 100 m derived from S-based ^{238}U lead to significant underestimation of ^{234}Th fluxes by an average of 20% and as high as 40% (Table 2). These differences in ^{234}Th fluxes will have direct consequences for ^{234}Th derived elemental fluxes such as C, N, P and trace metals.” This is a conclusion of the all section. I would thus move these sentences to the end of Section 3.1.

Response: fixed

Line 260: $S > 12$?

Response: It should be $S > 10$ as stated in the original text. McKee et al. (1987) and Swarzenski et al. (2004) looked at two different salinity thresholds in terms of the ^{238}U -S linear correlation.

Lines 276-277: Shepherd et al., 2017 is not listed in the section “References”.

Response: fixed

Line 308: For comparison, please give also the fraction of upwelled ^{234}Th fluxes compared to the total fluxes for the offshore stations.

Response: The fraction of upwelled ^{234}Th fluxes compared to total fluxes is now quoted in text.

Line 308: Cite Figure 5.

Response: quoted

Line 322: Mean ^{234}Th “activities” in the top layer.. ?

Response: fixed

Line 322: Please precise what does “top layer” exactly mean. Like in the caption of Figure 6 and Table 3..

Response: fixed

Line 355: cruises

Response: fixed

Lines 380 and 382: Maybe change the ^{234}Th activities into $^{234}\text{Th}/^{238}\text{U}$ ratios, as it might be easier to realise the magnitude of the deficit.

Response: The reviewer provided a very good suggestion here, but we unfortunately cannot proceed for one important reason: the activities of ^{238}U in Black et al. (2017) were not measured nor are they reported in the available GEOTRACES database.

Lines 411-412: And ^7Be isotopes, as you mention line 351.

Response: added

Line 696: Error bars “are” (instead of were) indicated. Shelf instead of nearshore (to keep the same wording all along the manuscript).

Response: fixed

Figure 2: It is difficult to see the small variations. Please, decrease the size of the ^{234}Th data points and make the lines thinner. Add the error bars. If they are already indicated but too small to be seen, please mention it in the caption. The x axes are always the same, please, keep the O_2 values only on the top of the figure and the ^{234}Th , ^{238}U , fluorescence values only on the bottom of the figure. By doing so, you can slightly increase the size of each graph. Please, keep your colour legend of Figure 1 and indicate the shelf to offshore transect by an arrow (maybe by writing W and E, like in Figure 5). Like in Black et al., 2018: indicate the depth of the mixed layer and the start of the Oxygen deficient zone.

Response: Figure 2 was modified according to most of these comments. The depth of the mixed layer is now indicated by a red dashed line. The start of the oxygen deficient zone is where oxygen diminishes. We did not use color legend from Figure 1 to keep Figure 2 clean and easy to read.

Figure 3: Please indicate the error bars. If it is too much for the figures, I recommend to at least, indicate the size of the average error bar on a corner of the plot. Indicated the O_2 concentrations in Figure 3c as well. This would confirm that the poor relationship does not depend on O_2 concentrations.

Response: We now added error bars, which are smaller than symbols. We also added oxygen concentrations in Figure 3c.

Figure 4: There is no need to write the depths for each plot. Write the values only on the left side of the figure. The legend has to be fixed and “fluorescence” has to be added on the bottom x axis of Figure 4c. In the legend of Figure 4a, define that the black dotted line corresponds to salinity and that the black solid line corresponds to temperature.

Response: We fixed the vertical axes and Figure 4c horizontal axis (now Figure 5). It is not correct regarding reviewer’s comment on the dashed and solid lines. We specified in the caption that the dashed lines corresponded to temperature and dashed lines corresponded to salinity.

Figure 5: I do like this Figure: it is clear. Please modify the caption and write “5-20m below ML” instead of “base of the ML. In the legend, please write “Final total ^{234}Th flux” for the white dots to keep the same wording than in Table 1.

Response: Fixed

Table 1: Please modify the caption and the top line of the 2nd column: “ ^{234}Th flux 5-20m below the ML” instead of “below the ML” or “at the base of the ML”.

Response: Fixed

Interactive comment on “Effects of ^{238}U variability and physical transport on water column ^{234}Th downward fluxes in the coastal upwelling system off Peru” by Ruifang Xie et al.

Anonymous Referee #2

5 Received and published: 16 April 2020

We thank the reviewer for his/her constructive comments. We’ve listed our point-by-point response in bold below.

10 Major comments This study evaluated the impact from the non-linearity of U-S relationship, temporal variability of ^{234}Th and 3-D physical transport of ^{234}Th on the estimation of downward ^{234}Th flux. I initially read the manuscript with interest but realized finally that I need to give it up. This is an important but difficult topic that has been ignored in various ^{234}Th studies, while the superficial description and discussion on the data by the authors keep the manuscript from further acceptance. The non-linearity between ^{238}U and salinity is interesting and I totally agree that will induce an over- or under-estimation on the final ^{234}Th flux. I feel very nerves that the authors attributed such non-linearity to the flooding and landslides without any obvious evidences shown in the manuscript. Meanwhile, if it was true that high uranium was transported from the coastal waters, then how was that for ^{234}Th ? I guess the ^{234}Th activity could be low in the same water, and including the low ^{234}Th water also elevated the ^{234}Th flux calculation.

Response: The coastal El Niño of 2017 induced coastal precipitation as strong as the 1997-98 El Niño (Echevin et al. 2008), resulting in devastating flooding and landslides in central and northern coastal Peru. Evidence of this coastal El Niño has been presented in earlier studies cited in our manuscript. This intense flooding likely delivered large amount of fresh water, dissolved and particulate ^{238}U , and possibly particulate ^{234}Th . ^{234}Th is highly particle reactive so it is unlikely that the coastal flooding has directly introduced dissolved ^{234}Th to the coastal water. ^{234}Th produced in-situ within the upper water column was likely scavenged quickly due to enhanced particulate input from land at this time. The addition of freshwater and riverine U may draw the datapoints up and down the conservative U-salinity mixing line (as shown in Owens et al. 2011). However, this was not the case in our study where majority of the U data points fall above the U-salinity line defined by Owens et al. (2011). We thus agreed with the reviewer that coastal flooding is unlikely the cause of such deviations. We now have significantly modified the discussion regarding the non-linear U-salinity correlation based on both reviewers’ comments to include U remobilization induced by bottom water oxygenation being one of the main

mechanisms for enhanced water column U. We have disregarded the discussion of coastal flooding being one of the main causes of the poor U-salinity correlation.

40 Echevin, V. M., Colas, F., Espinoza-Morriberon, D., Anculle, T., Vasquez, L., and Gutierrez, D.: Forcings and evolution of the 2017 coastal El Niño off Northern Peru and Ecuador, *Frontiers in Marine Science*, 5, 367, <https://doi.org/10.3389/fmars.2018.00367>, 2018.

45 Owens, S., Buesseler, K., and Sims, K.: Re-evaluating the ^{238}U -salinity relationship in seawater: Implications for the ^{238}U – ^{234}Th disequilibrium method, *Marine Chemistry*, 127, 31-39, <https://doi.org/10.1016/j.marchem.2011.07.005>, 2011.

The authors further examine the physical transport of ^{234}Th , but again the in-depth discussion will be required. Quite a few descriptions and explanations should be listed here: The methods on the upwelling rate estimation using wind stress and its uncertainty, the diffusivity using in situ microstructure measurements and the detail calculation for horizontal advection (the equation 3 showed in the manuscript is way too simple for this paper). I strongly recommend the authors to add these parts in the methods and discussion during the revision, and most importantly, the evaluation of the uncertainty and error should be carefully done. For example, the authors calculated the upwelling rate was on the order of 10^{-6} to 10^{-7} m s⁻¹, those values actually were quite low compared to other upwelling sites.

Response: We have expanded the Methods section to include essential details of how upwelling rates, current velocities and diffusivities were estimated. We did not include methods for error propagation in the Supplement/main text, but refer the readers to references of Resplandy et al., 2012 and Savoye et al., 2006 who illustrated the derivations in great details. In the Results section, we detailed ^{234}Th fluxes due to radioactive production and decay, advection and diffusion.

Upwelling rates off Peru estimated in our study were indeed smaller than some of the upwelling rates in other upwelling sites, but is in accord with the atmospheric and oceanic conditions off Peru at the time of sample collection. Wind stress were unusually weak off Peru beginning the last quarter of 2016 and lasted until the first half of March 2017. Toward the end of March 2017, an increase of the nearshore wind stress and a relaxation in offshore wind stress off northern Peru generated an intense wind stress curl anomaly and an associated downwelling (e.g., Echevin et al. 2008). An SST transect along 12°S off Peru showed that upwelling was restricted to the shelf and in the upper 50 m. These atmospheric and oceanic conditions were unique and resulted in very weak upwelling rates off Peru.

Lüdke, J., et al. (in review 2020). "Influence of intraseasonal eastern boundary circulation variability on hydrography and biogeochemistry off Peru." *Ocean Sci. Discuss.* 2019: 1-31.

Resplandy, L., Martin, A. P., Le Moigne, F., Martin, P., Aquilina, A., Mémery, L., Lévy, M., and Sanders, R.: How does dynamical spatial variability impact ^{234}Th -derived estimates of organic export?, *Deep Sea Research Part I: Oceanographic Research Papers*, **68**, 24-45, <https://doi.org/10.1016/j.dsr.2012.05.015>, 2012.

80 Savoye, N., Benitez-Nelson, C., Burd, A. B., Cochran, J. K., Charette, M., Buesseler, K. O., Jackson, G. A., Roy-Barman, M., Schmidt, S., and Elskens, M.: ^{234}Th sorption and export models in the water column: a review, *Marine Chemistry*, **100**, 234-249, <https://doi.org/10.1016/j.marchem.2005.10.014>, 2006.

85 In the last part of the discussion, the authors used a whole paragraph for the ^{234}Th residence time. I did not find any wordings on the detailed calculation method for those residence time. I guess they are estimated using an 1-D steady state model, but given that the physical transport was important for some stations as the authors had pointed out, 3-D estimation for the ^{234}Th residence time will also be needed.

90 **Response: We now included the formulation for estimation of residence time, which was based on a 1D steady state model. Although this 1D steady state model is an oversimplification of a multi-dimensional process and should be used with caution, it provides a good first order estimate for understanding the highly dynamic nature of the ^{234}Th residence time. It also provides a reasonable value that can be directly compared to**
95 **values estimated in earlier ^{234}Th flux studies that did not consider physical processes. We now added this discussion to the main text.**

100 The ^{234}Th and ^{238}U data obtained in the region could be very interesting, the detailed description of their profiles should be more interesting.

Response: We now included a Result section that describe both ^{234}Th and ^{238}U profiles in detail.

105 I think the authors should expand their methods part, and separate the result and discussion. In addition, I found some sentences in the conclusion should also move to the discussion.

Response: We now expanded the Methods part to include detail description on how upwelling rates, current velocities and diffusivities were calculated. We also separated the Results and Discussion.

110 I also have quite a few detailed comments listed below. Minor comments:

The title: Effects of ^{238}U variability and physical transport. It gave me an impression that the author is evaluating the ^{238}U transport which is actually ^{234}Th .

115 **Response: The manuscript looks into the roles of ^{238}U variability and physical transport on ^{234}Th distribution and transport, and we think that the title fully reflects the goals and findings of this manuscript.**

Page 3, Line 41, Add “in the upper ocean” after “export fluxes”

Response: fixed

120 Page 3, Line 47, Bhat et al., 1968 is not a appropriate reference, add some Santschi paper, and show the K_d values here.

Response: We disagree with the reviewer. Bhat et al. (1968) is one of the earlier field studies that have demonstrated the particle reactive nature of ^{234}Th in the ocean. We now added the K_d values with reference to Santschi et al. (2006).

125

Page 3, Line 50-51, ^{234}Th flux can be obtained even if you do not integrate with depth.

Response: It is necessary to integrate ^{234}Th activities with depth in order to estimate ^{234}Th flux.

130 Page 5, Methods part, Add the methods for the upwelling rate estimation, diffusivity calculation and current from ADCP.

Response: We added methods on how upwelling rates, current velocities and diffusivities were calculated

135 Page 6, Line 118-120, Did you just assume that ^{234}Th had been in equilibrium with ^{238}U or you would acidify those sample and let them stay for a year until the equilibrium would be reached. Please make that clearer.

Response: Only ^{238}U samples were acidified. We now clarified this in the manuscript.

140 Page 6, Line 125, 1 dpm or 10 dpm?

Response: It is 1 dpm as stated in the text.

Page 6, Line 125, what was the volume of your sample? 4L or 2L.

Response: We now specified 4L as the sample volume.

145

Page 8, Line 171-172, Show the detailed calculation methods here or in the supplements. I guess here involved the simplification and manipulation of your data.

Response: We now added details in the Methods section on how upwelling velocities, current velocities, and diffusivities were calculated. We also added details on how vertical and horizontal gradients were calculated.

150

Page 9, Line 180-181, I have concerned on the ADCP-data which are snapshots data during the cruise, while ^{234}Th is a chemical tracer with a time integrated information included. How do you match the different time scale between the two parameters?

Response: We appreciate the reviewer's concerned. As stated in Lines 226 in the revised manuscript, "Data collected at the same positions 226 within 5 days due to station repeats were also included in the velocity average." In another word, the ADCP-derived current velocities were averaged over a 5-day timescale. This timescale is somewhat shorter than the residence time of ^{234}Th . But given the short cruise timeframe, we consider this time averaged appropriate.

160

Page 10, Line 208, Separation between results and discussion could be better.

Response: We now separated results and discussion.

165 Page 11, Line 221-231, The detailed description of ^{234}Th and ^{238}U activities, ranges, averages, and their relationship with Chl a and oxygen will be appreciated.

Response: We added detailed descriptions in the new Results section.

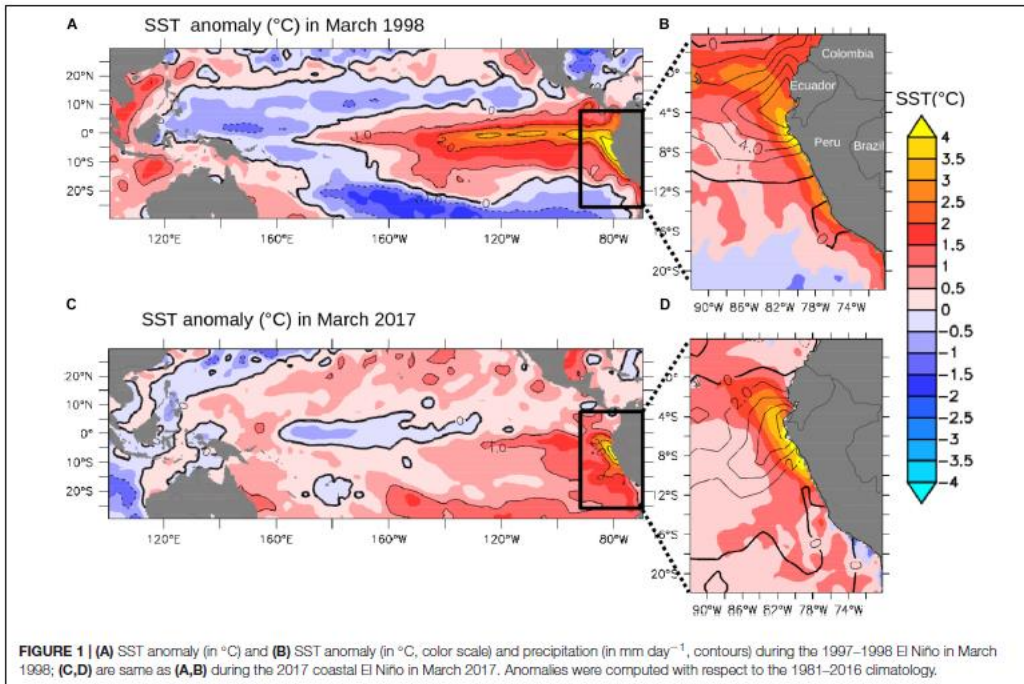
Page 13, Line 265-267, How about ^{234}Th ?

170 **Response: Unlike U, Th is not redox sensitive.**

Page 13, Line 268-273, This is too superficial? Do you have any optics data here?

Response: Numerous evidences of the 2017 coastal El Niño off Peru has been published in previous studies, which were referenced in our manuscript.

175 Here we referenced to a figure by Echevin et al. (2018) who showed that the magnitude of precipitation in the eastern equatorial Pacific during the 2017 coastal El Niño was almost as intense as that during the 1997-98 El Niño event:



180 Page 14, Line 290-295, Show the equation for NSS calculation. I think in the supplement you will also need to explain how you do the error propagation.

Response: We now referenced readers to Resplandy et al. (2012) and Savoye et al. (2006) for details regarding the derivation of NSS flux formulation and error propagation.

185 Page 14, Line 303, How reliable is your upwelling rate? I do not believe those numbers. Show the methods and put more discussion here.

Response: We now showed details in the Methods section how we calculated the upwelling rates. Please also refer to our response above in Line 53-58 in this document, which we showed that the upwelling rates estimated in our study were reliable.

190

Page 15, Line 318, How much is “trivial”? less than 10

Response: We now specified it as “insignificant, ranging between 1% and 10%” instead of “trivial”.

195 Page 15, Line 325, How do you calculate the ^{234}Th gradient?

Response: We grouped stations within a 1° by 1° grid and calculated the average ^{234}Th for the top layer, and large scale (1° apart) horizontal ^{234}Th gradients were calculated based on this grouping. We now added details in the Results section on how vertical and horizontal gradients were calculated.

200

Page 16-17, Line 353-355, The time scale for the methods is very different.

Response: Agreed. We now specified these two methods estimate upwelling rates at different timescales.

205 Page 17, Line 370, How do you do the calculation? 1D steady state? Or 3D steady State?

Response: Please refer to our response in Line 70-76 in this document.

Page 19, Line 411-414, not related, or move to discussion part.

Page 19, Line 417-420, Move to discussion part?

210 **Response to both comments: Both are relevant in terms of implications for future coastal ^{234}Th flux studies.**

The references: all numbers of molecular weight for the isotopes should be in the upper case. There are quite a few errors on the references, please do the careful check.

215 **Response: fixed**

Figures: I think adding some figures here will be much helpful. Please add a transect distribution for ^{238}U and ^{234}Th to show the coast to offshore difference. And also add some profiles of the vertical diffusivity should be better.

220 **Response: We now added a figure of $^{234}\text{Th}/^{238}\text{U}$ transects to show the distributions of shelf-offshore ^{234}Th deficits (as Figure 3 in the revised manuscript). Diffusivity profiles were shown in the original supplementary file.**

Figure 1: It is better to put the current field here in the map, or show it in a separate figure?

225 **Response: We now added the current field in Figure 1.**

Figure 2: Show the MLD and bottom depths here

Response: We now indicated the MLD for all stations (red dashed lines) and bottom depths for stations whose bottom depths are shallower than 600 m (scale of y-axis).

230

Figure 4, Can you show the profiles of ^{234}Th for stations 458 and 508, although the surface sample was missing.

Response: We now showed the comparison between stations 458 and 508 in Figure 4 (Figure 5 in the revised manuscript).

1 (Mark-up version: Changes made in the revision were marked with an
2 underline.)

3 **Effects of ^{238}U variability and physical transport on water column
4 ^{234}Th downward fluxes in the coastal upwelling system off Peru**

5
6 Ruifang C. Xie^{1*}, Frédéric A. C. Le Moigne², Insa Rapp¹, Jan Lüdke¹, Beat Gasser³, Marcus
7 Dengler¹, Volker Liebetrau¹, Eric P. Achterberg¹

8
9 ¹GEOMAR Helmholtz Center for Ocean Research Kiel, Wischhofstrasse 1-3, 24148 Kiel,
10 Germany

11 ²Mediterranean Institute of Oceanography (UM 110, MIO), CNRS, IRD, Aix Marseille
12 Université, Marseille, France

13 ³IAEA Environment Laboratories, 4 Quai Antoine 1er, 98000 Monaco
14 Monaco

15

16 * corresponding author: rxie@geomar.de

17 **Abstract**

18 The eastern boundary region of the southeastern Pacific Ocean hosts one of the world's most
19 dynamic and productive upwelling systems with an associated oxygen minimum zone (OMZ).
20 The variability in downward export fluxes in this region, with strongly varying surface
21 productivity, upwelling intensities and water column oxygen content, is however poorly
22 understood. Thorium-234 (^{234}Th) is a powerful tracer to study the dynamics of export fluxes of
23 carbon and other elements, yet intense advection and diffusion in nearshore environments impact
24 the assessment of depth-integrated ^{234}Th fluxes when not properly evaluated. Here we use
25 VmADCP current velocities, satellite wind speed and *in situ* microstructure measurements to
26 determine the magnitude of advective and diffusive fluxes over the entire ^{234}Th flux budget at 25
27 stations from 11°S to 16°S in the Peruvian OMZ. Contrary to findings along the GEOTRACES
28 P16 eastern section, our results showed that weak surface wind speed during our cruises induced
29 low upwelling rates and minimal upwelled ^{234}Th fluxes, whereas vertical diffusive ^{234}Th fluxes
30 were important only at a few shallow shelf stations. Horizontal advective and diffusive ^{234}Th
31 fluxes were negligible because of small alongshore ^{234}Th gradients. Our data indicated a poor
32 correlation between seawater ^{238}U activity and salinity. Assuming a linear relationship between
33 the two would lead to significant underestimations of the total ^{234}Th flux by up to 40% in our
34 study. Proper evaluation of both physical transport and variability in ^{238}U activity is thus crucial
35 in coastal ^{234}Th flux studies. Finally, we showed large temporal variations on ^{234}Th residence
36 times across the Peruvian upwelling zone, and cautioned future carbon export studies to take
37 these temporal variabilities into consideration while evaluating carbon export efficiency.

38 **Keywords:** eastern tropical South Pacific, ^{234}Th tracer, uranium-salinity correlation, physical
39 processes, residence time

40 1. Introduction

41 Isotopes of thorium (Th) are widely used as tracers for particle cycling in the oceans
42 (Waples et al., 2006). In particular, ^{234}Th has been extensively used to trace particle dynamics and
43 export fluxes in the upper ocean, and to quantify the marine budgets of important macro- and
44 micronutrients such as carbon (C), nitrogen (N), phosphorus (P) and iron (Fe) (Bhat et al., 1968;
45 Buesseler et al., 1992; Coale and Bruland, 1987; Lee et al., 1998; Le Moigne et al., 2013;
46 Cochran and Masqué, 2003; Van Der Loeff et al., 2006; Black et al., 2019). ^{234}Th has a relatively
47 short half-life ($\tau_{1/2} = 24.1$ days) that allows studies of biological and physical processes occurring
48 on timescales of days to weeks. Unlike its radioactive parent uranium-238 (^{238}U , $\tau_{1/2} = 4.47$ Ga)
49 that is soluble in seawater, ^{234}Th is highly particle reactive with a particle-water partition
50 coefficient of 10^3 to 10^8 (Santschi et al., 2006 and references therein) and thus strongly scavenged
51 by particles (Bhat et al., 1968). Generally, a deficit of ^{234}Th relative to ^{238}U is observed in the
52 surface ocean and reflects net removal of ^{234}Th due to particle sinking, whereas secular
53 equilibrium between ^{234}Th and ^{238}U is observed for intermediate and deep waters. Integrating this
54 surface ^{234}Th deficit with depth yields the sinking flux of ^{234}Th and, if elemental: ^{234}Th ratios are
55 known, the sinking flux of elements such as C, N, P, and trace metals (Bhat et al., 1968;
56 Buesseler et al., 1998; Buesseler et al., 1992; Coale and Bruland, 1987; Weinstein and Moran,
57 2005; Buesseler et al., 2006; Owens et al., 2015; Black et al., 2019; Puigcorbé et al., 2020).

58 Various ^{234}Th models have been put forward to study adsorption/desorption, aggregation
59 and export, but single box models that assume negligible ^{234}Th fluxes due to physical transport
60 are commonly used to calculate oceanic ^{234}Th -derived particle fluxes (see detailed review by
61 Savoye et al., 2006). This assumption is typically appropriate in open ocean settings where ^{234}Th
62 fluxes due to advection and diffusion are small relative to the downward fluxes of ^{234}Th

63 associated with particle sinking. However, in upwelling regions such as the equatorial Pacific and
64 coastal systems, advective and diffusive ^{234}Th fluxes may become increasingly important (e.g.,
65 Bacon et al., 1996; Buesseler et al., 1998; Buesseler et al., 1995; Dunne and Murray, 1999). For
66 example, in the equatorial Pacific, strong upwelling post El-Niño could account for ~50% of the
67 total ^{234}Th fluxes (Bacon et al., 1996; Buesseler et al., 1995). Ignoring the upwelling term could
68 thus lead to an underestimation of ^{234}Th fluxes by a factor of 2. Conversely, horizontal diffusion
69 carrying recently upwelled, ^{234}Th -replete waters has been shown to balance the upwelled ^{234}Th
70 fluxes in the central equatorial Pacific (Dunne and Murray, 1999). To the contrary, advective and
71 diffusive ^{234}Th fluxes were minimal off the Crozet Islands in the Southern Ocean due to limited
72 horizontal ^{234}Th gradients, long residence time of water masses, and low upwelling rates and
73 diffusivities (Morris et al., 2007).

74 The dynamic nature of coastal processes requires that physical terms be included in ^{234}Th
75 flux calculation whenever possible. Accurate measurements of current velocities and diffusivities
76 are however challenging and thus direct observations of the effects of physical processes on ^{234}Th
77 distributions in coastal regions are scarce. Limited studies have incorporated advection and
78 diffusion in the nearshore zones of the Arabian Sea (Buesseler et al., 1998), Gulf of Maine
79 (Gustafsson et al., 1998; Benitez-Nelson et al., 2000), the South China Sea (Cai et al., 2008) and
80 Peruvian oxygen minimum zone (OMZ) (Black et al., 2018). In the Arabian Sea, coastal
81 upwelling during the southwest monsoon season could account for over 50% of the total ^{234}Th
82 flux (Buesseler et al., 1998). Horizontal advection has been shown to be substantial in the Inner
83 Cosco Bay of the Gulf of Maine (Gustafsson et al., 1998), whereas offshore advection and
84 diffusion are only important in late summer (Benitez-Nelson et al., 2000). Therefore, the
85 importance of physical processes on the ^{234}Th flux estimate is highly dependent on the seasonal
86 and spatial variability of the current velocities, diffusivities and ^{234}Th gradients. In terms of the

87 Peruvian OMZ, Black et al. (2018) showed that coastal upwelling accounts for >50% of total
88 ^{234}Th fluxes at 12°S; however, how upwelling ^{234}Th fluxes vary seasonally and spatially in this
89 region is unclear.

90 Another uncertainty in ^{234}Th flux calculations in such region stems from variations on
91 dissolved ^{238}U activities. Generally speaking, U behaves conservatively under open ocean oxic
92 conditions and is linearly correlated with salinity (Chen et al., 1986; Ku et al., 1977; Owens et al.,
93 2011). However, numerous studies have shown that such correlation breaks down in various
94 marine environments including the tropical Atlantic (Owens et al., 2011), Mediterranean Sea
95 (Schmidt and Reyss, 1991), and Arabian Sea (Rengarajan et al., 2003). Although it is generally
96 accepted that deviations from the linear ^{238}U -S correlation will lead to differences in the final
97 calculated ^{234}Th fluxes, there is currently little knowledge on how significant these differences
98 could be.

99 In this study, we report vertical profiles of ^{234}Th and ^{238}U along four transects
100 perpendicular to the coastline of Peru (i.e. shelf-offshore transects). We evaluate the ^{238}U -S
101 correlation in low-oxygen waters and how deviations from this correlation impact final ^{234}Th flux
102 estimates. We also assess the spatial and temporal importance of advection and diffusion on ^{234}Th
103 flux estimates.

104

105 **2. Sampling and methods**

106 2.1 Seawater sampling and analysis

107 Seawater samples were collected at 25 stations along 4 shelf-offshore transects between
108 11°S and 16°S in the Peruvian OMZ during two cruises M136 and M138 on board the RV

109 Meteor (Figure 1). Cruise M136 took place in austral autumn (April 11 to May 3, 2017) along
110 two main transects at 12°S and 14°S (Dengler and Sommer, 2017). Two stations from M136
111 (stations 458 and 495) were reoccupied within a week (repeat stations 508 and 516, respectively)
112 to evaluate the steady-state assumption in the ^{234}Th flux calculation. The surface sample of the
113 repeat station 508 (reoccupied 4.5 days after station 458) was missing so only results from repeat
114 stations 495 and 516 (occupation interval 1.5 days) were compared and discussed in terms of the
115 non-steady state model (section 3.3). ^{234}Th sampling during cruise M138 was carried out in
116 austral winter (June 1 to July 4, 2017) and focused on four shelf-offshore transects at 11°S, 12°S,
117 14°S and 16°S.

118 At each station, a stainless-steel rosette with Niskin bottles (Ocean Test Equipment®) was
119 deployed for sampling of total ^{234}Th in unfiltered seawater and dissolved ^{238}U (0.2 μm pore size,
120 Acropak® polycarbonate membrane). High vertical resolution sampling was performed in the
121 upper 200 m where most of the biological activity occurs; additional depths were sampled down
122 to 600 m, or 50 m above the seafloor. Deep seawater at 1000 m, 1500 m, and 2000 m was
123 sampled at three stations to determine the absolute β counting efficiency. Salinity, temperature,
124 oxygen concentrations and fluorescence data (Table S1) were derived from the sensors (Seabird
125 Electronics® 9plus system) mounted on the CTD frame (Krahmann, 2018; Lüdke et al., in review
126 2020).

127 Sample collection and subsequent chemical processing and analysis for total ^{234}Th
128 followed protocols by Pike et al. (2005) and SCOR Working Group RiO5 cookbook
129 (<https://cmer.who.edu/>). Briefly, a ^{230}Th yield tracer (1 dpm) was added to each sample (4 L)
130 before Th was extracted with MnO_2 precipitates. Precipitates were filtered onto 25 mm quartz
131 microfiber filters (Whatman® QMA, 2.2 μm nominal pore size) and dried overnight at 50°C, after
132 which they were counted at sea on a Risø® low-level beta GM multiscaler until uncertainty was

133 below 3%, and again 6 months later at home laboratory for background ^{234}Th activities. After the
134 second beta counting, filters were digested in an 8M HNO_3 /10% H_2O_2 solution (Carl Roth[®], trace
135 metal grade). 10 dpm of ^{229}Th was added to each sample at the beginning of digestion to achieve
136 a 1:1 atom ratio between ^{229}Th : ^{230}Th . Digested samples were diluted in a 2.5% HNO_3 /0.01% HF
137 mixture and $^{229}\text{Th}/^{230}\text{Th}$ ratios were measured using an ICP-MS (ThermoFisher[®] Element XR) to
138 determine the chemistry yield and final ^{234}Th activities. The average yield was calculated to be
139 $97\% \pm 6\%$ ($n = 247$). For a subset of samples (marked in Table S1) whose analysis failed during
140 initial ICP-MS measurement, anion chromatography (Biorad[®] AG1x8, 100 – 200 mesh, Poly-
141 Prep columns) was performed to remove Mn from the sample matrix before another ICP-MS
142 analysis. This subset of samples also included three samples (marked in Table S1) whose initial
143 ICP-MS measurement was successful, to test whether anion chromatography affects final ICP-
144 MS results. Identical $^{229}\text{Th}/^{230}\text{Th}$ ratios were measured for samples with and without column
145 chromatography (see Table S1 footnotes for details).

146 Each ^{238}U sample was acidified to pH ~1.6 at sea and transported home for analysis.
147 Samples of dissolved ^{238}U were diluted 20 times in 1N HNO_3 at home laboratory and spiked with
148 an appropriate amount of ^{236}U spike to achieve ^{236}U : $^{238}\text{U} \sim 1:1$. Ratios of ^{236}U : ^{238}U were analyzed
149 by ICP-MS (ThermoFisher Element XR) and activities of ^{238}U were calculated using isotope
150 dilution. Seawater certified reference materials (CRMs), CASS-6 and NASS-7, and the
151 International Association for the Physical Sciences of the Oceans (IAPSO) standard seawater
152 were analyzed routinely for uranium concentrations.

153

154 2.2 Flux calculation

155 Assuming a one box model, the temporal change of ^{234}Th activities is balanced by
 156 production from ^{238}U , radioactive decay of ^{234}Th , removal of ^{234}Th onto sinking particles, and
 157 transport into or out of the box by advection and diffusion (Bhat et al., 1968; Savoye et al., 2006;
 158 and references therein):

$$159 \quad \frac{\partial A_{Th}}{\partial t} = \lambda(A_U - A_{Th}) - P + V \quad (1)$$

160 where A_U and A_{Th} are respectively the activities of dissolved ^{238}U and total ^{234}Th , λ is the
 161 decay constant of ^{234}Th , P is the net removal flux of ^{234}Th , and V is the sum of advective and
 162 diffusive fluxes. It is recommended that the time interval between station occupations should
 163 be >2 weeks in order to adequately capture the temporal variability of the mean spatial gradients
 164 rather than small local changes (Resplandy et al., 2012). The solution of Eq. (1) (Savoye et al.,
 165 2006) is

$$166 \quad P = \lambda \left[\frac{A_U(1-e^{-\lambda\Delta t}) + A_{Th1} \cdot e^{-\lambda\Delta t} - A_{Th2}}{1 - e^{-\lambda\Delta t}} \right] \quad (2)$$

167 where Δt is the time interval between repeat occupations of a station; A_{Th1} and A_{Th2} are
 168 respectively total ^{234}Th activities during the first and second occupation. At times when repeat
 169 sampling is not possible within adequate cruise timeframe, steady state conditions are generally
 170 assumed, i.e. $\frac{\partial A_{Th}}{\partial t} = 0$. In this case, Eq. (1) is simplified into:

$$171 \quad P = \int_0^z \lambda(A_U - A_{Th})dz + V \quad (3)$$

172 The vertical flux of ^{234}Th , P ($\text{dpm m}^{-2} \text{d}^{-1}$), is integrated to the depth of interest. Earlier
 173 studies generally used arbitrarily fixed depths (e.g., the base of mixed layer or ML, and 100 m)
 174 for ^{234}Th and POC flux estimates (e.g., Bacon et al., 1996; Buesseler et al., 1992). Recent studies
 175 emphasized the need to normalize POC flux to the depth of euphotic zone (EZ), which separates

176 the particle production layer in the surface from the flux attenuation layer below (Black et al.,
 177 2018; Buesseler and Boyd, 2009; Rosengard et al., 2015). In the open ocean, the depth of EZ is
 178 generally similar to ML depth. The PAR (Photosynthetically Active Radiation) sensor was not
 179 available during both of our cruises, so that it was not possible to identify the base of the EZ. For
 180 the purpose of this study, the slight difference of the exact depth chosen (ML vs. EZ) was of little
 181 relevance to the significance of physical processes and ^{238}U variability.

182

183 2.3 Quantification of the physical fluxes

184 The physical term V in Eq. (2) is expressed as following:

$$185 \quad V = \int_0^z \left(w \frac{\partial Th}{\partial z} - u \frac{\partial Th}{\partial x} - v \frac{\partial Th}{\partial y} \right) dz + \int_0^z \left(K_x \frac{\partial^2 Th}{\partial x^2} + K_y \frac{\partial^2 Th}{\partial y^2} - K_z \frac{\partial^2 Th}{\partial z^2} \right) dz \quad (3)$$

186 where w is the vertical (i.e. upwelling) velocity (m s^{-1}), u and v respectively the zonal and
 187 meridional current velocities (m s^{-1}), and K_x , K_y , and K_z represent eddy diffusivities ($\text{m}^2 \text{s}^{-1}$) in
 188 zonal, meridional and vertical directions, respectively. $\frac{\partial Th}{\partial z}$, $\frac{\partial Th}{\partial x}$ and $\frac{\partial Th}{\partial y}$ are vertical and horizontal
 189 ^{234}Th gradients ($\text{dpm L}^{-1} \text{m}^{-1}$), and $\frac{\partial^2 Th}{\partial x^2}$, $\frac{\partial^2 Th}{\partial y^2}$ and $\frac{\partial^2 Th}{\partial z^2}$ are respectively the second derivative of
 190 ^{234}Th ($\text{dpm L}^{-1} \text{m}^{-2}$) on the zonal, meridional and vertical directions.

191

192 2.3.1 Estimation of upwelling velocities

193 In the Mauritanian and Peruvian coastal upwelling regions, there is strong evidence that
 194 upwelling velocities in the mixed layer derived from satellite scatterometer winds and Ekman
 195 divergence (Gill, 1982) agree well with those from helium isotope disequilibrium (Steinfeldt et

196 al., 2015). The parameterization by Gill (1982) considers the baroclinic response of winds
197 blowing parallel to a coastline in a two-layer ocean. Vertical velocity (w) at the interface yields

198
$$w = \frac{\tau}{\rho f a} e^{-x/a} \quad (4)$$

199 where τ is the wind stress ($\text{kg m}^{-1} \text{s}^{-2}$) parallel to the coast line, ρ the water density (kg m^{-3}),
200 f the Coriolis parameter (s^{-1}), a the first baroclinic Rossby radius (km) and X the distance (km)
201 to the coast.

202 Upwelling velocities were calculated at stations within 60 nautical miles (nm) of the
203 coast, where upwelling is the most significant (Steinfeldt et al., 2015). We used $a = 15$ km for all
204 stations based on the results reported by Steinfeldt et al. (2015) for the same study area. The
205 magnitude of monthly wind stress was estimated from the monthly wind velocities (Smith, 1988):

206
$$\tau = \rho_{air} C_D U^2 \quad (5)$$

207 where ρ_{air} is the air density above the sea surface (1.225 kg m^{-3}), C_D the drag coefficient
208 (10^{-3} for wind speed $< 6 \text{ m s}^{-1}$), and U the wind speed.

209 Monthly wind speed (m s^{-1}) fields from MetOp-A/ASCAT scatterometer sensor with a
210 spatial resolution of 0.25° (Bentamy and Croize-Fillon, 2010) were retrieved from the Centre de
211 Recherche et d'Exploitation Satellitaire (CERSAT), at IFREMER, Plouzané (France) (data
212 version numbers L3-MWF-GLO-20170903175636-01.0 and L3-MWF-GLO-20170903194638-
213 01.0). We assumed a linear decrease of w from base of the mixed layer toward both the ocean
214 surface and 240 m depth (bottom depth of our shallowest station). Upwelling rates at any depth
215 between 0 and 240 m at individual station could thus be determined once w was estimated.
216 Following (Rapp et al., 2019), an error of 50% was assigned to estimated upwelling velocities to

217 account for uncertainties associated with the spatial structure and temporal variability of the wind
218 field, and the satellite wind product near the coast.

219

220 2.3.2 Estimation of upper-ocean velocities

221 During both cruises a phased-array vessel-mounted acoustic Doppler current profiler
222 (VmADCP; 75 kHz Ocean Surveyor, Teledyne RD-Instruments) continuously measured zonal
223 and meridional velocities in the upper 700 m of the water column (Lüdke et al., in review 2020).
224 Post-processing of the velocity data included water track calibration and bottom editing. After
225 calibration, remaining uncertainty of hourly averages of horizontal velocities are smaller than 3
226 cm s⁻¹ (e.g. Fischer et al., 2003). For the horizontal advective flux calculation (Eq. 3), velocities
227 collected within a 10 km radian at inshore stations (St. 353, 428, 458, 475, 508, 904, and 907)
228 and within a 50 km radian at offshore stations were averaged. Data collected at the same positions
229 within 5 days due to station repeats were also included in the velocity average. As representative
230 for the near-surface flow, we extracted the velocity data from the top 30 m for M136 stations and
231 top 50 m for M138 station; these depths correspond to 5-20 m below the base of the ML during
232 each cruise.

233

234 2.3.3 Estimation of vertical and horizontal eddy diffusivities

235 While the strength of ocean turbulence determines the magnitude of diapycnal or vertical
236 eddy diffusivities, the intensity of meso- and submesoscale eddies determine the magnitude of
237 lateral eddy diffusivities. During the R/V Meteor cruise M136 and the follow up cruise in the
238 same region, the strength of upper-ocean turbulence was measured using shear probes mounted to

239 a microstructure profiler. The loosely-tethered profiler was optimized to sink at a rate of 0.55 m s⁻¹
240 and equipped with three shear sensors, a fast-response temperature sensor, an acceleration
241 sensor, two tilt sensors and conductivity, temperature, depth sensors sampling with a lower
242 response time. At most CTD stations 3 to 9 microstructure profiles were collected. Standard
243 processing procedures were used to determine the dissipation rate of turbulent kinetic energy (ϵ)
244 in the water column (see Schafstall et al., 2010 for detailed description). Subsequently, turbulent
245 vertical diffusivities K_z were determined from $K_z = \Gamma \epsilon N^{-2}$ (Osborn, 1980), where N is
246 stratification and Γ is the mixing efficiency for which a value of 0.2 was used following Gregg et
247 al. (2018). The 95% confidence intervals for averaged K_z values were determined from Gaussian
248 error propagation following Schafstall et al. (2010).

249 Altogether, 189 microstructure profiles were collected during M136 (Thomsen and
250 Lüdke, 2018) and 258 profiles during the follow-up cruise M137 (unpublished data; May 6 – 29,
251 2017). An average turbulent vertical diffusivity profile was calculated from all inshore (<500m
252 water depth) and from all offshore (>500m water depth) profiles (Figure S1). Microstructure
253 profiles collected during cruise M138 were not available but there were little variations amongst
254 the cruise average inshore and offshore microstructure profiles from M136 and M137 despite
255 drastic change in the intensities of the poleward Peru Chile Undercurrent (Lüdke et al., in review
256 2020). It thus appears appropriate to apply these average vertical diffusivities also to stations
257 during M138.

258 Horizontal eddy diffusivity could not be determined from data collected during the
259 cruises. Surface eddy diffusivities in the North Atlantic OMZ were estimated to be on the order of
260 a few 1000 m² s⁻¹ that decrease exponentially with depth (Hahn et al., 2014). Similar magnitude
261 of eddy diffusivities was estimated for the ETSP based on surface drifter data and satellite

262 altimetry (Abernathy and Marshall, 2013; Zhurbas and Oh, 2004). We thus consider an eddy
263 diffusivity of $1000 \text{ m}^2 \text{ s}^{-1}$ as a good approximate in this study for the evaluation of horizontal
264 diffusive ^{234}Th fluxes.

265

266 2.4 Residence time of ^{234}Th

267 The residence time ($\tau_{1/2}$) of total ^{234}Th represents a combination of the time required for
268 the partition of dissolved ^{234}Th onto particulate matter and that for particle removal. In a one-box
269 model, the residence time of an element of interest can be estimated by determining the standing
270 stock of this element and the rates of elemental input to the ocean or the rate of element removal
271 from seawater to sediments (Bewers and Yeats, 1977; Zimmerman, 1976):

$$272 \quad \tau_{1/2} = \frac{A_{Th(mean)} \cdot Z}{P} \quad (6)$$

273 For the case of ^{234}Th , $A_{Th(mean)}$ is the averaged ^{234}Th activities of the surface layer, Z is the
274 depth of surface layer, and P the removal flux of ^{234}Th .

275

276 **3. Results**

277 3.1 Profiles of dissolved ^{238}U , total ^{234}Th , oxygen and fluorescence

278 The vertical profiles of ^{238}U and ^{234}Th activities are shown in Figure 2 and tabulated in
279 Table S1. Data from station 508 were reported in Figure 2 and Table S1 but excluded in the
280 Discussion section, because the surface sample at 5 m from this station was missing, which
281 prevents any flux calculation. Also tabulated in Table S1 are temperature, salinity and

282 concentrations of oxygen and fluorescence obtained from the CTD sensors. Uranium
283 concentrations of CRMs and the IAPSO standard seawater are reported in Table S2.

284 Activities of ^{238}U showed small to negligible variations with depth, averaging 2.54 ± 0.05
285 dpm L^{-1} (or $3.28 \pm 0.07 \text{ ng/g}$, 1SD, $n = 247$) at all stations. The vertical distributions of ^{238}U did
286 not appear to be affected by water column oxygen concentrations or the extent of surface Chl a
287 (Figure 2). Average U concentrations of both CASS-6 ($2.77 \pm 0.04 \text{ ng g}^{-1}$, 1SD, $n = 5$) and
288 NASS-7 ($2.86 \pm 0.05 \text{ ng/g}$, 1SD, $n = 5$) measured in this study agreed well with certified values
289 ($2.86 \pm 0.42 \text{ ng g}^{-1}$ and $2.81 \pm 0.16 \text{ ng g}^{-1}$, respectively). Average ^{238}U concentration measured in
290 our IAPSO standard seawater (OSIL batch P156) ($3.24 \pm 0.06 \text{ ng g}^{-1}$, 1SD, $n = 27$) is slightly
291 higher than that reported in Owens et al. (2011) ($3.11 \pm 0.03 \text{ ng g}^{-1}$, 1SD, $n = 10$, OSIL P149),
292 and may reflect slight differences in U concentrations between different OSIL batches.

293 Total ^{234}Th varied from 0.63 to 2.89 dpm L^{-1} (Figure 2). All stations showed large ^{234}Th
294 deficits in surface waters with $^{234}\text{Th}/^{238}\text{U}$ ratios as low as 0.25 (Figure 3). The extent of surface
295 ^{234}Th deficits did not vary as a function of depths of either mixed layer or the upper oxic-anoxic
296 interface, nor the magnitude of surface fluorescence concentrations (Table 1, Figure 2). ^{234}Th at
297 all stations generally reached equilibrium with ^{238}U at depths between 30 m and 250 m. The
298 equilibrium depths were slightly shallower toward the shelf at the 11°S , 12°S and 16°S transects.
299 At St. 912, deficits of ^{234}Th extended beyond 600 m depth (Figure 2). The following stations (St.
300 428, 879, 898, 906, 907, 915, 919) displayed a secondary ^{234}Th deficit below the equilibrium
301 depth, indicative of ^{234}Th removal processes. A small ^{234}Th excess at depth was only observed for
302 St. 559 at 100 m. Ratios of $^{234}\text{Th}/^{238}\text{U}$ for deep samples at 1000 m, 1500 m, and 2000 m varied
303 between 0.95 and 1.02 (1.00 ± 0.04 , 1SD, $n = 11$), suggesting that ^{234}Th was at equilibrium with
304 ^{238}U at these depths.

305

306 3.2 Vertical and horizontal ^{234}Th gradients

307 Discrete vertical ^{234}Th gradients in each profile (or the curvature of the profile) were
308 estimated by the difference in ^{234}Th activities and that in sampling depths. As such, vertical ^{234}Th
309 gradients varied greatly amongst stations, and were larger at shallow depths ranging from 0.003
310 dpm L⁻¹ m⁻¹ to 0.085 dpm L⁻¹ m⁻¹ (median 0.013 dpm L⁻¹ m⁻¹). Vertical ^{234}Th gradients were
311 essentially negligible at and below equilibrium depths.

312 While calculation of the vertical ^{234}Th gradient is straightforward, the same is hardly true
313 for the determination of horizontal ^{234}Th gradient. Here we consider the top layer as top 30 m
314 during M136 and top 50 m during M138. Mean ^{234}Th activities in the top layer of the water
315 column are highly variable amongst stations (Table 3, Figure 4), and likely reflect variations
316 occurring at small temporal and spatial scales in the Peruvian OMZ. Quantification of the
317 horizontal ^{234}Th gradient between individual station thus may not be adequate to evaluate large
318 scale advection and eddy diffusion across the study area. Therefore, alongshore ^{234}Th gradients
319 on a larger spatial scale (1° apart) were instead calculated by grouping stations into 1° by 1° grids
320 and averaging ^{234}Th activities of each grid for the top layer. Alongshore ^{234}Th gradients in the top
321 layer at nearshore stations for M138 are fairly consistent, ranging from 1.5×10^{-6} dpm L⁻¹ m⁻¹ to
322 1.7×10^{-6} dpm L⁻¹ m⁻¹, with a slightly stronger gradient in the north compared to the south. The
323 net difference in alongshore ^{234}Th gradient is merely 2×10^{-7} dpm L⁻¹ m⁻¹. A slightly smaller
324 alongshore ^{234}Th gradient of 4.8×10^{-7} dpm L⁻¹ m⁻¹ was observed for M136. The magnitude of the
325 net difference in alongshore ^{234}Th gradient for M136 cannot be adequately quantified, due to
326 smaller spatial sampling coverage. Judging on the similarity in the spatial distributions of mean

327 ^{234}Th between cruises M136 and M138, it is reasonable to assume that net difference in
328 alongshore ^{234}Th gradient remained similar during both cruises.

329

330 3.3 Steady state vs. non-steady state models

331 The relative importance of ^{234}Th fluxes due to advection and diffusion were assessed here
332 assuming steady state conditions, which assume negligible temporal ^{234}Th variability. But how
333 valid is this assumption in the Peruvian upwelling zone? Profiles of temperature and oxygen at
334 repeat stations 458 and 508 showed that a lightly cooler and oxygen-depleted water mass
335 dominated at the upper 50 m at station 508 (Figure 5). However, an assessment of the ^{234}Th
336 fluxes at these two stations were not possible as the surface sample from station 508 was missing.
337 Repeat stations 495 and 516 show substantial temporal variations in ^{234}Th activities at each
338 sampled depth in the top 200 m, while temperature and salinity profiles confirmed that similar
339 water masses were sampled during both occupations (Figure 5). Particularly, the surface ^{234}Th
340 deficit was more intense at St. 495 ($^{234}\text{Th}/^{238}\text{U} = 0.44$) compared to St. 516 ($^{234}\text{Th}/^{238}\text{U} = 0.73$).
341 Correspondingly, ^{234}Th fluxes decreased substantially from St. 495 to St. 516. At 100 m, the
342 difference in ^{234}Th fluxes between these two stations was $\sim 30\%$ ($3200 \pm 90 \text{ dpm m}^{-2} \text{ d}^{-1}$ at St.
343 495 and $2230 \pm 110 \text{ dpm m}^{-2} \text{ d}^{-1}$ at St. 516). At 200 m where ^{234}Th resumed equilibrium with ^{238}U
344 at both stations, ^{234}Th flux difference was $\sim 25\%$ ($4510 \pm 220 \text{ dpm m}^{-2} \text{ d}^{-1}$ at St. 495 and $3455 \pm$
345 $200 \text{ dpm m}^{-2} \text{ d}^{-1}$ at St. 516). Taking the non-steady state term in Eq. (1) into consideration (see
346 details in Resplandy et al. (2012) and Savoye et al. (2006) for the derivation of flux formulation
347 and error propagation) increased total ^{234}Th at St. 516 by 40% to $3110 \pm 1870 \text{ dpm m}^{-2} \text{ d}^{-1}$ at 100
348 m (or 45% to $5040 \pm 2290 \text{ dpm m}^{-2} \text{ d}^{-1}$ at 200 m), which is indistinguishable within error from
349 fluxes at St. 495. The large errors associated with the non-steady state calculation prevent a

350 meaningful application of this model in the current study (also see discussion in Resplandy et al,
351 2012). As estimation of the physical fluxes is independent of the models chosen between steady
352 and non-steady states, the following results and discussion sections regarding physical effects on
353 the ^{234}Th flux estimates is based on the steady state model only.

354

355 3.4 Export fluxes of ^{234}Th

356 Fluxes of ^{234}Th due to radioactive production and decay (hereafter ‘production flux’),
357 upwelling, and vertical diffusion were reported in Table 1 and Figure 6 for both depths 5-20 m
358 below the ML and at 100 m. Due to sampling logistics, we did not sample at the base of the ML,
359 but 5-20 m below the ML. This depth corresponded closely to the EZ depth used in Black et al.
360 (2018) in the same study area during austral summer 2013. For the purpose of comparison with
361 earlier studies which reported ^{234}Th fluxes at 100 m, we also calculated ^{234}Th fluxes at 100 m in
362 this study. The production fluxes of ^{234}Th at 5-20 m below the ML ranged from $560 \text{ dpm m}^{-2} \text{ d}^{-1}$
363 to $1880 \text{ dpm m}^{-2} \text{ d}^{-1}$, whereas at 100 m they were much higher at $850 \text{ dpm m}^{-2} \text{ d}^{-1}$ to 3370 dpm m^{-2}
364 d^{-1} . There is no discernable trend regarding the production fluxes between the shelf and offshore
365 stations, similar to those seen along the eastern GP16 transect (Black et al. 2017).

366 Alongshore winds were unusually weak off Peru preceding and during our sampling
367 campaign as a result of the 2017 coastal El Niño (Echevin et al., 2018; Lüdke et al., in review
368 2020; Peng et al., 2019), which resulted in nominal upwelling in the water column. At nearshore
369 stations, upwelling rates at the base of the ML varied between $1.3 \times 10^{-7} \text{ m s}^{-1}$ and $9.7 \times 10^{-6} \text{ m s}^{-1}$
370 $^{-1}$, whereas upwelling rates at offshore stations were on the order of $10^{-10} \text{ m s}^{-1}$ to 10^{-8} m s^{-1} and
371 essentially negligible. As a result, upwelled ^{234}Th fluxes at 5-20 m below the ML were only
372 significant at stations closest to shore; these stations were $428 (130 \text{ dpm m}^{-2} \text{ d}^{-1})$, $883\text{-}12 (80 \text{ dpm}$

373 $\text{m}^{-2} \text{d}^{-1}$) and 904-16 ($280 \text{ dpm m}^{-2} \text{d}^{-1}$) whose upwelled ^{234}Th fluxes accounted for 10%, 11% and
374 25% of the total ^{234}Th fluxes respectively (Figure 6). Upwelled ^{234}Th fluxes at the rest of the
375 stations accounted for less than 2% of the total ^{234}Th fluxes (6% at stations 353 and 907-11) and
376 were insignificant. At 100 m, both vertical ^{234}Th gradients and upwelling rates were significantly
377 smaller compared to shallower depths. As a result, upwelled ^{234}Th fluxes were less than 70 dpm
378 $\text{m}^{-2} \text{d}^{-1}$, or less than 4% of total ^{234}Th fluxes.

379 Similarly, vertical diffusivities, shown as running mean over 20 m in Figure S1, were an
380 order of magnitude higher at shallow stations ($3.2 \times 10^{-4} \pm 1.7 \times 10^{-4} \text{ m}^2 \text{ s}^{-1}$; 1SD, 27 m to 100 m
381 below sea surface) compared to those at deep stations ($1.7 \times 10^{-5} \pm 0.6 \times 10^{-5} \text{ m}^2 \text{ s}^{-1}$; 1SD; 34 –
382 100 m below sea surface). Within the 27 m to 33 m layer at deep stations, vertical diffusivities
383 decreased exponentially by an order of magnitude within a few meters; below this depth, vertical
384 diffusivities remained relatively stable (Figure S1). This is not surprising as wind-driven
385 turbulent is most significant at the ocean surface (Buckingham et al., 2019). In this study, the
386 sampling depths immediately below the ML were generally 30 m and 60 m. A few high vertical
387 diffusivity values around 30 m at deep stations were unlikely representative for the 30 m – 60 m
388 water column layer. We thus opted to only apply vertical diffusivities below 33 m at deep
389 stations. Relative standard errors (RSE) associated with diffusivity estimates varied from 35% to
390 55%. Vertical diffusive ^{234}Th fluxes at 5-20 m below the ML, determined using both vertical
391 diffusivity and vertical ^{234}Th gradient, varied greatly amongst stations. At shallow stations 428,
392 458, and 883-12, vertical diffusive ^{234}Th fluxes made up 37% ($490 \text{ dpm m}^{-2} \text{d}^{-1}$), 14% (160 dpm
393 $\text{m}^{-2} \text{d}^{-1}$), and 21% ($160 \text{ dpm m}^{-2} \text{d}^{-1}$) of total ^{234}Th fluxes, respectively (Figure 6). At the rest of
394 the stations, vertical diffusive ^{234}Th fluxes appeared to be insignificant, ranging between 1% and
395 10% in the total ^{234}Th flux budget. At 100 m, vertical diffusive ^{234}Th fluxes at station 428, 458,

396 and 883-12 remained high at 390 dpm m⁻² d⁻¹, 150 dpm m⁻² d⁻¹, 120 dpm m⁻² d⁻¹, respectively,
397 whereas those at the rest of the stations accounted for < 2% of the total ²³⁴Th flux.

398 Horizontal advective and diffusive ²³⁴Th fluxes were both very small. Average alongshore
399 current velocities (Lüdke et al., in review 2020) for the surface layer varied from 0.06 m s⁻¹ to
400 0.34 m s⁻¹. At the peripheral of a freshly-formed anticyclonic eddy (St. 915-1), alongshore current
401 velocities could be as high as 0.53 m s⁻¹. Taking the mean alongshore velocity of 0.2 m s⁻¹ and the
402 net difference in alongshore ²³⁴Th gradient of 2 x 10⁻⁷ dpm L⁻¹ m⁻¹, the resulting net horizontal
403 advective ²³⁴Th flux is ~ 50 dpm m⁻² d⁻¹, a mere 3-9% of the total ²³⁴Th fluxes.

404 Horizontal diffusive ²³⁴Th flux was estimated using an average eddy diffusivity of 1000
405 m² s⁻¹ (see Methods section 2.3.3) and the alongshore ²³⁴Th gradient. A maximum value of 10
406 dpm m⁻² d⁻¹ was calculated, which accounted for <1% of total ²³⁴Th flux at all stations. Note that
407 the horizontal advective and lateral diffusive fluxes presented here are a rough estimate and
408 should only provide an idea of their order of magnitude. Due to the uncertainty inherent to the
409 estimates, we refrain from adding these values to Table 1.

410

411 **4. Discussion**

412 4.1 Lack of linear ²³⁸U – salinity correlation in the Peruvian OMZ

413 The water column profiles of ²³⁸U in the Peruvian OMZ (Figure 2) are similar to those
414 seen in the open ocean (see compilations in Owens et al., 2011 and Van Der Loeff et al. (2006),
415 and references therein). It thus appears that water column suboxic/anoxic conditions alone is not
416 sufficient to remove U, in contrast to sedimentary U studies underlying low oxygen waters where
417 soluble U(VI) diffused downward into subsurface sediments and reduced to insoluble U(IV)

418 (Anderson et al., 1989; Böning et al., 2004; Scholz et al., 2011). Our inference is in accord with
419 water column ^{238}U studies in intense OMZs in the eastern tropical North Pacific (Nameroff et al.,
420 2002) and the Arabian Sea (Rengarajan et al., 2003), where ^{238}U concentrations remain constant
421 over the entire upper water column studied.

422 Dissolved ^{238}U and salinity across the entire Peruvian OMZ displayed poor linear
423 correlation regardless of seawater oxygen concentrations (Figure 7a-b). The general consensus is
424 that U behaves conservatively in oxic seawater in the open ocean and early observations have
425 shown that ^{238}U activities can be calculated from salinity based on a simple linear correlation
426 between the two (e.g. Chen et al., 1986; Ku et al., 1977). Recent compilations in Van Der Loeff et
427 al. (2006) and Owens et al. (2011) further demonstrated that the majority of uranium data points
428 in the global seawater dataset follow a linear correlation with seawater salinity. The ^{238}U -salinity
429 formulations from either Chen et al. (1986) or Owens et al. (2011) are thus generally appropriate
430 for open ocean conditions and have been widely used in ^{234}Th flux studies. However, this linear
431 ^{238}U -salinity correlation breaks down in the Peruvian OMZ. Furthermore, the measured ^{238}U
432 activities in this study correlated poorly with those calculated from salinity using the Owens
433 formulation regardless of water column oxygen concentrations (Table S2, Figure 7c), with the
434 former significantly higher than the projected values and differences up to 10%. Both evidences
435 suggested that non-conservative processes have introduced significant amount of dissolved U into
436 the water column.

437 It is likely that this poor ^{238}U -salinity correlation in the water column is not a unique
438 feature off the coast of Peru. Poor correlations between dissolved ^{238}U and salinity have been
439 previously observed in open ocean settings such as the Arabian Sea (Rengarajan et al., 2003) and
440 the Pacific Ocean (Ku et al., 1977), and shelf-estuary systems such as the Amazon shelf (McKee

441 et al., 1987; Swarzenski et al., 2004). It is possible that the narrow range of salinity within any
442 single ocean basin precludes a meaningful ^{238}U -salinity correlation (Ku et al., 1977; Owens et al.,
443 2011). For the Peruvian shelf system, two possible scenarios may further explain the lack of
444 linear ^{238}U -salinity correlation in the water column. Firstly, authigenic U within the sediments
445 may be remobilized under ENSO-related oxygenation events. Pore water and bottom water
446 geochemistry measurements during two previous cruises (M77-1 and M77-2) along an 11°S
447 transect off Peru showed large diffusive fluxes of U out of the Peruvian shelf sediments despite
448 that both Fe reduction and U reduction took place in the top centimeters of sediments (Scholz et
449 al., 2011). It was suggested that a minute increase in bottom water oxygen concentration induced
450 by El Niño events would be sufficient in shifting the U(VI)/U(IV) boundary by a few centimeters
451 and remobilize authigenic U (Scholz et al., 2011). Preceding and during our sampling campaign,
452 a coastal El Niño event, with coastal precipitation as strong as the 1997-98 El Niño event, had
453 developed rapidly and unexpectedly in January, and disappeared by May 2017 during cruise
454 M136 (Echevin et al., 2018; Garreaud, 2018; Peng et al., 2019). This strong coastal El Niño event
455 could induce an oxygenation event large enough to remobilized authigenic U along the Peruvian
456 shelf. Secondly, resuspension of bottom sediments and subsequent desorption of U from ferric-
457 oxyhydroxides could affect the ^{238}U -salinity relationship, similar to that seen on the Amazon
458 shelf at salinity above 10 (McKee et al., 1987) and in laboratory experiments (Barnes and
459 Cochran, 1993). Fe reduction and release from the Peruvian shelf sediments (Noffke et al., 2012;
460 Scholz et al., 2014) could release additional U to overlying waters. The magnitude of such,
461 however, has not been quantified.

462 The consequence of the notable difference between measured ^{238}U in this study and
463 salinity-based ^{238}U to ^{234}Th flux according to Eq. (2) is neither linear nor straightforward, because
464 the vertical gradients of both ^{238}U and ^{234}Th strongly affects the impacts of ^{238}U variations on

465 ^{234}Th fluxes. In this study, ^{234}Th fluxes at 100 m derived from salinity-based ^{238}U lead to
466 significant underestimation of ^{234}Th fluxes by an average of 20% and as high as 40% (Table 2).
467 These differences in ^{234}Th fluxes will have direct consequences for ^{234}Th derived elemental fluxes
468 such as C, N, P and trace metals. It is thus important to note that U concentrations in coastal
469 systems are highly sensitive to bottom water oxygen concentrations and redox-related U addition,
470 variability of which is expected to intensify with future climate change (Shepherd et al., 2017).
471 Relatively minor variations in dissolved ^{238}U could account for substantial
472 overestimation/underestimation of the depth-integrated ^{234}Th fluxes. We thus encourage future
473 ^{234}Th flux studies in such environments to include seawater ^{238}U analysis.

474

475 4.2 Dynamic advective and diffusive ^{234}Th fluxes

476 The significance of advection and diffusion in the total ^{234}Th flux budget highly depends
477 on the upwelling rate, current velocity, vertical diffusivity, and ^{234}Th gradient on the horizontal
478 and vertical directions. Our results demonstrated that physical processes off Peru during and post
479 the 2017 coastal El Nino have very limited impact on the downward fluxes of ^{234}Th (Figure 6).

480 Our findings are in reasonable agreement with those from the GEOTRACES GP16
481 eastern section along 12°S from Peru to Tahiti, in which Black et al. (2018) quantified both
482 horizontal and vertical advective ^{234}Th fluxes. Horizontal advective fluxes for the upper 30 m
483 water column estimated during GP16 were $\sim 180 \text{ dpm m}^{-2} \text{ d}^{-1}$ for all nearshore and offshore
484 stations, similar in magnitude to those estimated in our study. Upwelling fluxes along GP16
485 eastern section was suggested to account for 50% to 80% of total ^{234}Th fluxes at the base of the
486 euphotic zone (at similar depths or slightly deeper than ML depths in the current study) (Black et
487 al., 2018). Total ^{234}Th fluxes along the GP16 eastern section, ranging from 4000 to 5000 dpm m^{-2}

488 d^{-1} at the base of the euphotic zone, were much higher than those in our study (560 to 1900 dpm
489 $m^{-2} d^{-1}$ at the base of the ML). This difference could be related to the period of sampling (austral
490 autumn and winter 2017 in our study vs. austral summer 2013 for the GP16 section). We note that
491 the estimated vertical mixing rates based on 7Be isotope at the base of the euphotic zone along the
492 GP16 section (Kadko, 2017) were at least an order of magnitude higher than the upwelling rates
493 at the base of the ML at nearby stations in our study. This difference could stem from different
494 methods used to estimate upwelling rates at different timescales, and may also reflect the
495 dynamic upwelling system off Peru in which upwelling rates vary greatly seasonally and
496 interannually. During cruises M136 and M138, upwelling favorable easterly winds off Peru were
497 weak, resulting in negligible coastal upwelling. Coastal upwelling in the same general area was
498 also suggested to be negligible in austral summer 2013 during cruise M92 due to nominal surface
499 wind stress (Thomsen et al., 2016). Results from studies conducted in the same year (October to
500 December 2013, Kadko, 2017; December 2012, Steinfeldt et al., 2015) indicate that seasonal
501 upwelling rates vary drastically in the Peruvian upwelling zone. The seasonal dynamics of coastal
502 upwelling off Peru are similar to those seen in the Arabian Sea, where large upwelled ^{234}Th fluxes
503 only occurred during mid-late southwest monsoon at stations close to shore (Buesseler et al.,
504 1998). Our findings lend further support to earlier studies that advection and diffusion are
505 seasonally important for ^{234}Th fluxes in regions with high upwelling velocities and diffusivities
506 such as the equatorial Pacific (Bacon et al., 1996; Buesseler et al., 1995; Dunne and Murray,
507 1999) and coastal sites such as the Arabian Sea (Buesseler et al., 1998) and offshore Peru (Black
508 et al., 2018; this study).

509

510 4.3 Residence time of ^{234}Th in the Peruvian OMZ

511 The residence time calculated using equation (6) was based on a simplified one-dimension
512 (1D) model of Zimmerman (1976). This 1D steady state model is obviously an oversimplification
513 of a multi-dimensional process, it however provides a good first order estimate for understanding
514 the highly dynamic nature of the ^{234}Th residence time. It also provides a reasonable value that can
515 be directly compared to values estimated in earlier ^{234}Th flux studies that did not consider the
516 physical processes. Furthermore, we showed in the Discussion (sections 4.2) that physical
517 processes, namely upwelling and vertical diffusion, are only important at a few shelf stations. We
518 thus consider this simple 1D model robust in estimating the residence time of total ^{234}Th .

519 In this study, residence time of total ^{234}Th in the surface layer (top 30 m during M136 and
520 top 50 m during M138) varied from 20 days at shallow stations to 95 days at deep stations (mean
521 $\tau = 51 \pm 23$ days, 1SD, $n = 24$; Table 3). These values were similar to those estimated within the
522 California Current (Coale and Bruland, 1985) and the residence times of particulate organic
523 carbon (POC) and nitrogen (PON) (Murray et al., 1989), but were much longer than predicted in
524 nearshore shelf waters where residence times of total ^{234}Th were on the order of a few days
525 (Kaufman et al., 1981; Kim et al., 1999; and references therein). The longer residence times
526 estimated in our study could reflect a combination of weak surface ^{234}Th deficits ($^{234}\text{Th} = 0.63$ to
527 1.82 dpm L^{-1}) (Figure 3) and low export fluxes (800 to 2000 dpm $\text{m}^{-2} \text{d}^{-1}$, Figure 7). Nearshore
528 seawater samples during GP16 (Black et al., 2018) featured similar surface ^{234}Th deficits ($^{234}\text{Th} =$
529 0.63 to 1.33 dpm L^{-1}) but much higher downward ^{234}Th fluxes (4000 to 5000 dpm $\text{m}^{-2} \text{d}^{-1}$) as a
530 result of strong upwelling, implying that residence times of total ^{234}Th in the Peruvian OMZ
531 during GP16 occupation would be 3 – 6 times shorter. Indeed, a quick re-assessment of the GP16
532 data predicted a shorter residence time of total ^{234}Th of 5 – 23 days within the euphotic zone of
533 the coastal Peruvian OMZ.

534 These temporal variations on the residence times of total ^{234}Th have important
535 implications for the estimation of POC fluxes and quantification of carbon export efficiency.
536 Firstly, seasonal changes in Th residence times reflect variations in particle removal over
537 different integrated timescales. For example, POC produced in surface waters during GP16
538 (austral summer 2013) (Black et al., 2018) would have been exported out of the euphotic zone 3-
539 6 times faster than it did during austral autumn 2017 (this study). Secondly, to properly evaluate
540 carbon export efficiency, surface net primary production (NPP) should be averaged over a similar
541 timescale as the residence time of total ^{234}Th during station occupation. Applying a 16-day
542 averaged NPP for export efficiency estimate (Black et al., 2018; Henson et al., 2011) would likely
543 not be appropriate in the current study in which total ^{234}Th fluxes integrated timescales of several
544 weeks. ^{234}Th residence times should thus be properly quantified in coastal studies before deriving
545 export efficiencies over varying NPP integration timescales.

546

547 **5. Conclusions and implications for coastal ^{234}Th flux studies**

548 Advection and diffusion are important in coastal and upwelling regions with respect to
549 ^{234}Th export fluxes (Bacon et al., 1996; Buesseler et al., 1995; Dunne and Murray, 1999;
550 Buesseler et al., 1998). Our findings show that their significance is subject to the seasonal
551 variability of the current and upwelling velocities, diffusivities and ^{234}Th gradients, and should be
552 evaluated on a case-to-case basis. Advective fluxes are perhaps the most straightforward to
553 estimate as current velocities can be obtained routinely from shipboard ADCP measurements and
554 upwelling rates calculated from satellite wind stress (Steinfeldt et al., 2015; Bacon et al., 1996).
555 Horizontal and vertical velocities derived from general ocean circulation models also provide a
556 good first order estimate for advective ^{234}Th fluxes; this approach has been successfully

557 demonstrated in a few studies (Buesseler et al., 1995; Buesseler et al., 1998). In addition, the
558 anthropogenic SF₆ tracer and radium isotopes, widely used to quantify nutrient and Fe fluxes
559 (Charette et al., 2007; Law et al., 2001), as well as ⁷Be isotope (Kadko, 2017), could be used
560 independently to constrain horizontal and vertical exchange rates of ²³⁴Th (Morris et al., 2007;
561 Charette et al., 2007; Buesseler et al., 2005). When *in situ* microstructure measurements are
562 available (this study), vertical diffusivity can be directly calculated to estimate the vertical
563 diffusive ²³⁴Th fluxes. Yet, microstructure analysis is not a routine measurement on
564 oceanographic cruises. Earlier studies in the equatorial Pacific and the Gulf of Maine have shown
565 that general ocean circulation models and a simple assumption on dissipation coefficients could
566 provide a robust estimate on vertical and horizontal diffusivities (Benitez-Nelson et al., 2000;
567 Gustafsson et al., 1998; Charette et al., 2001). Therefore, the calculation of physical fluxes is
568 possible, though challenging, and ²³⁴Th fluxes due to physical processes should be carefully
569 considered when conducting research in a coastal and upwelling systems.

570 A striking finding in this study is that the assumption of a linear ²³⁸U-salinity correlation
571 could lead to one of the largest errors in ²³⁴Th flux estimates. In our study, using the salinity-
572 based ²³⁸U activities resulted in significant underestimation of total ²³⁴Th fluxes by as much as
573 40%. Because the translation of ²³⁸U activities to ²³⁴Th fluxes is not linear, larger differences
574 between measured and salinity-based ²³⁸U do not necessarily contribute to greater overestimation
575 or underestimation of ²³⁴Th fluxes. For example, moderate difference of 3-6% in ²³⁸U throughout
576 the upper 100 m at station 898 lead to 40% difference in final ²³⁴Th flux, while a 5-9% difference
577 in ²³⁸U at station 906 only resulted in 16% ²³⁴Th flux difference (Table 2, S2). We would thus
578 stress the importance of ²³⁸U measurements in future ²³⁴Th flux studies particularly in coastal and
579 shelf regions.

580 Finally, our study showed that the residence times of total ^{234}Th in the Peruvian nearshore
581 waters varied seasonally. Tropical OMZs are important hotspots for carbon sequestration from the
582 atmosphere and enhanced sedimentary carbon preservation (Arthur et al., 1998; Suess et al.,
583 1987). These OMZs are projected to intensify as a result of future climate change (Keeling and
584 Garcia, 2002; Schmidtko et al., 2017; Stramma et al., 2008). Future studies should take into
585 consideration the large temporal variations of the residence times of total ^{234}Th in order to
586 properly evaluate how carbon biogeochemical cycles and carbon export efficiency in these
587 OMZs will respond to continuing ocean deoxygenation,

588

589 **Data availability**

590 Data are available in supplementary tables and will be archived in Pangea upon
591 publication of the article.

592

593 **Author contribution**

594 RCX, FACLM and EAP designed the study. RCX carried out sampling, on-board beta
595 counting of ^{234}Th , and drafted the manuscript. IR conducted ^{234}Th and ^{238}U analyses at home
596 laboratory. JL computed current velocities and vertical diffusivities respectively from VmADCP
597 and microstructure profiler data. All co-authors had a chance to review the manuscript and
598 contributed to discussion and interpretation of the data presented.

599

600 **Competing interests**

601 The authors declare that they have no conflict of interest.

602

603 **Acknowledgements**

604 We thank the crew and science party on board M136 and M138 for their help in sample collection
605 and instrument operation. Thank you to SiaoJean Ko, Dominik Jasinski, André Mutzberg and
606 Mario Esposito for their laboratory assistance. We thank two anonymous reviewers and the
607 associate editor, Marilaure Grégoire, for their constructive comments. The project, cruises, IR, JL
608 and RCX were funded by the German SFB 754 program (‘Climate-Biogeochemistry Interactions
609 in the Tropical Ocean’), and FACLM by a DFG Fellowship of the Excellence Cluster “The
610 Future Ocean” (CP1403). This manuscript benefited from stimulating discussions at the
611 BIARRITZ (‘bridging international activity and related research into the twilight zone’)
612 workshop held in Southampton, UK in 2019.

References

- 613
614
615 Abernathey, R. P., and Marshall, J.: Global surface eddy diffusivities derived from satellite
616 altimetry, *Journal of Geophysical Research: Oceans*, 118, 901-916,
617 <https://doi.org/10.1002/jgrc.20066>, 2013.
- 618 Anderson, R. F., Fleisher, M. Q., and LeHuray, A. P.: Concentration, oxidation state, and
619 particulate flux of uranium in the Black Sea, *Geochimica et Cosmochimica Acta*, 53, 2215-2224,
620 [https://doi.org/10.1016/0016-7037\(89\)90345-1](https://doi.org/10.1016/0016-7037(89)90345-1), 1989.
- 621 Arthur, M. A., Dean, W. E., and Laarkamp, K.: Organic carbon accumulation and preservation in
622 surface sediments on the Peru margin, *Chemical Geology*, 152, 273-286,
623 [https://doi.org/10.1016/S0009-2541\(98\)00120-X](https://doi.org/10.1016/S0009-2541(98)00120-X), 1998.
- 624 Bacon, M., Cochran, J., Hirschberg, D., Hammar, T., and Flier, A.: Export flux of carbon at the
625 equator during the EqPac time-series cruises estimated from ^{234}Th measurements, *Deep Sea*
626 *Research Part II: Topical Studies in Oceanography*, 43, 1133-1153, [https://doi.org/10.1016/0967-](https://doi.org/10.1016/0967-0645(96)00016-1)
627 [0645\(96\)00016-1](https://doi.org/10.1016/0967-0645(96)00016-1), 1996.
- 628 Barnes, C. E., and Cochran, J. K.: Uranium geochemistry in estuarine sediments: Controls on
629 removal and release processes, *Geochimica et Cosmochimica Acta*, 57, 555-569,
630 [https://doi.org/10.1016/0016-7037\(93\)90367-6](https://doi.org/10.1016/0016-7037(93)90367-6), 1993.
- 631 Benitez-Nelson, C. R., Buesseler, K. O., and Crossin, G.: Upper ocean carbon export, horizontal
632 transport, and vertical eddy diffusivity in the southwestern Gulf of Maine, *Continental Shelf*
633 *Research*, 20, 707-736, [https://doi.org/10.1016/S0278-4343\(99\)00093-X](https://doi.org/10.1016/S0278-4343(99)00093-X), 2000.
- 634 Bentamy, A., and Croize-Fillon: Gridded surface wind fields from Metop/ASCAT measurements,
635 *International Journal of Remote Sensing*, doi:10.1080/01431161.2011.600348, 2010.
- 636 Bewers, J., and Yeats, P.: Oceanic residence times of trace metals, *Nature*, 268, 595-598, 1977.

637 Bhat, S., Krishnaswamy, S., Lal, D., and Moore, W.: $^{234}\text{Th}/^{238}\text{U}$ ratios in the ocean, Earth and
638 Planetary Science Letters, 5, 483-491, [https://doi.org/10.1016/S0012-821X\(68\)80083-4](https://doi.org/10.1016/S0012-821X(68)80083-4), 1968.

639 Black, E. E., Buesseler, K. O., Pike, S. M., and Lam, P. J.: ^{234}Th as a tracer of particulate export
640 and remineralization in the southeastern tropical Pacific, Marine Chemistry, 201, 35-50,
641 <https://doi.org/10.1016/j.marchem.2017.06.009>, 2018.

642 Black, E. E., Lam, P. J., Lee, J. M., and Buesseler, K. O.: Insights From the $^{238}\text{U} - ^{234}\text{Th}$ Method
643 Into the Coupling of Biological Export and the Cycling of Cadmium, Cobalt, and Manganese in
644 the Southeast Pacific Ocean, Global Biogeochemical Cycles, 33, 15-36,
645 <https://doi.org/10.1029/2018GB005985>, 2019.

646 Böning, P., Brumsack, H.-J., Böttcher, M. E., Schnetger, B., Kriete, C., Kallmeyer, J., and
647 Borchers, S. L.: Geochemistry of Peruvian near-surface sediments, Geochimica et Cosmochimica
648 Acta, 68, 4429-4451, <https://doi.org/10.1016/j.gca.2004.04.027>, 2004.

649 Buckingham, C. E., Lucas, N. S., Belcher, S. E., Rippeth, T. P., Grant, A. L. M., Le Sommer, J.,
650 Ajayi, A. O., and Naveira Garabato, A. C.: The Contribution of Surface and Submesoscale
651 Processes to Turbulence in the Open Ocean Surface Boundary Layer, Journal of Advances in
652 Modeling Earth Systems, 11, 4066-4094, <https://doi.org/10.1029/2019MS001801>, 2019.

653 Buesseler, K., Ball, L., Andrews, J., Benitez-Nelson, C., Belostock, R., Chai, F., and Chao, Y.:
654 Upper ocean export of particulate organic carbon in the Arabian Sea derived from thorium-234,
655 Deep Sea Research Part II: Topical Studies in Oceanography, 45, 2461-2487,
656 [https://doi.org/10.1016/S0967-0645\(98\)80022-2](https://doi.org/10.1016/S0967-0645(98)80022-2), 1998.

657 Buesseler, K. O., Bacon, M. P., Cochran, J. K., and Livingston, H. D.: Carbon and nitrogen
658 export during the JGOFS North Atlantic Bloom Experiment estimated from $^{234}\text{Th}: ^{238}\text{U}$
659 disequilibria, Deep Sea Research Part A. Oceanographic Research Papers, 39, 1115-1137,
660 [https://doi.org/10.1016/0198-0149\(92\)90060-7](https://doi.org/10.1016/0198-0149(92)90060-7), 1992.

661 Buesseler, K. O., Andrews, J. A., Hartman, M. C., Belostock, R., and Chai, F.: Regional estimates
662 of the export flux of particulate organic carbon derived from thorium-234 during the JGOFS
663 EqPac program, Deep Sea Research Part II: Topical Studies in Oceanography, 42, 777-804,
664 [https://doi.org/10.1016/0967-0645\(95\)00043-P](https://doi.org/10.1016/0967-0645(95)00043-P), 1995.

665 Buesseler, K. O., Andrews, J., Pike, S. M., Charette, M. A., Goldson, L. E., Brzezinski, M. A.,
666 and Lance, V.: Particle export during the southern ocean iron experiment (SOFEX), Limnology
667 and Oceanography, 50, 311-327, <https://doi.org/10.4319/lo.2005.50.1.0311>, 2005.

668 Buesseler, K. O., Benitez-Nelson, C. R., Moran, S., Burd, A., Charette, M., Cochran, J. K.,
669 Coppola, L., Fisher, N., Fowler, S., and Gardner, W.: An assessment of particulate organic carbon
670 to thorium-234 ratios in the ocean and their impact on the application of ^{234}Th as a POC flux
671 proxy, Marine Chemistry, 100, 213-233, <https://doi.org/10.1016/j.marchem.2005.10.013>, 2006.

672 Buesseler, K. O., and Boyd, P. W.: Shedding light on processes that control particle export and
673 flux attenuation in the twilight zone of the open ocean, Limnology and Oceanography, 54, 1210-
674 1232, <https://doi.org/10.4319/lo.2009.54.4.1210>, 2009.

675 Cai, P., Chen, W., Dai, M., Wan, Z., Wang, D., Li, Q., Tang, T., and Lv, D.: A high - resolution
676 study of particle export in the southern South China Sea based on ^{234}Th : ^{238}U disequilibrium,
677 Journal of Geophysical Research: Oceans, 113, 2008.

678 Charette, M. A., Moran, S. B., Pike, S. M., and Smith, J. N.: Investigating the carbon cycle in the
679 Gulf of Maine using the natural tracer thorium 234, Journal of Geophysical Research: Oceans,
680 106, 11553-11579, <https://doi.org/10.1029/1999JC000277>, 2001.

681 Charette, M. A., Gonnee, M. E., Morris, P. J., Statham, P., Fones, G., Planquette, H., Salter, I.,
682 and Garabato, A. N.: Radium isotopes as tracers of iron sources fueling a Southern Ocean
683 phytoplankton bloom, Deep Sea Research Part II: Topical Studies in Oceanography, 54, 1989-
684 1998, <https://doi.org/10.1016/j.dsr2.2007.06.003>, 2007.

685 Chen, J., Edwards, R. L., and Wasserburg, G. J.: ^{238}U , ^{234}U and ^{232}Th in seawater, Earth and
686 Planetary Science Letters, 80, 241-251, [https://doi.org/10.1016/0012-821X\(86\)90108-1](https://doi.org/10.1016/0012-821X(86)90108-1), 1986.

687 Coale, K. H., and Bruland, K. W.: ^{234}Th : ^{238}U disequilibria within the California Current 1,
688 Limnology and Oceanography, 30, 22-33, <https://doi.org/10.4319/lo.1985.30.1.0022>, 1985.

689 Coale, K. H., and Bruland, K. W.: Oceanic stratified euphotic zone as elucidated by ^{234}Th : ^{238}U
690 disequilibria 1, Limnology and Oceanography, 32, 189-200,
691 <https://doi.org/10.4319/lo.1987.32.1.0189>, 1987.

692 Cochran, J., and Masqué, P.: Short-lived U/Th series radionuclides in the ocean: tracers for
693 scavenging rates, export fluxes and particle dynamics, Reviews in Mineralogy and geochemistry,
694 52, 461-492, <https://doi.org/10.2113/0520461>, 2003.

695 Dengler, M., and Sommer, S.: Coupled benthic and pelagic oxygen, nutrient and trace metal
696 cycling, ventilation and carbon degradation in the oxygen minimum zone of the Peruvian
697 continental margin (SFB 754): Cruise No. M 136 11.04.–03.05. 2017 Callao (Peru)–Callao
698 Solute-Flux Peru I, METEOR-Berichte, 10.3289/CR_M136, 2017, 2017.

699 Dunne, J. P., and Murray, J. W.: Sensitivity of ^{234}Th export to physical processes in the central
700 equatorial Pacific, Deep Sea Research Part I: Oceanographic Research Papers, 46, 831-854,
701 [https://doi.org/10.1016/S0967-0637\(98\)00098-3](https://doi.org/10.1016/S0967-0637(98)00098-3), 1999.

702 Echevin, V. M., Colas, F., Espinoza-Morriberon, D., Anculle, T., Vasquez, L., and Gutierrez, D.:
703 Forcings and evolution of the 2017 coastal El Niño off Northern Peru and Ecuador, Frontiers in
704 Marine Science, 5, 367, <https://doi.org/10.3389/fmars.2018.00367>, 2018.

705 Fischer, J., Brandt, P., Dengler, M., Müller, M., and Symonds, D.: Surveying the upper ocean
706 with the Ocean Surveyor: a new phased array Doppler current profiler, Journal of Atmospheric
707 and Oceanic Technology, 20, 742-751, https://doi.org/10.1175/1520-
708 0426(2003)20<742:STUOWT>2.0.CO;2, 2003.

709 Garreaud, R. D.: A plausible atmospheric trigger for the 2017 coastal El Niño, International
710 Journal of Climatology, 38, e1296-e1302, <https://doi.org/10.1002/joc.5426>, 2018.

711 Gregg, M., D'Asaro, E., Riley, J., and Kunze, E.: Mixing efficiency in the ocean, Annual review
712 of marine science, 10, 443-473, 10.1146/annurev-marine-121916-063643, 2018.

713 Gustafsson, Ö., Buesseler, K. O., Rockwell Geyer, W., Bradley Moran, S., and Gschwend, P. M.:
714 An assessment of the relative importance of horizontal and vertical transport of particle-reactive
715 chemicals in the coastal ocean, Continental Shelf Research, 18, 805-829,
716 [https://doi.org/10.1016/S0278-4343\(98\)00015-6](https://doi.org/10.1016/S0278-4343(98)00015-6), 1998.

717 Hahn, J., Brandt, P., Greatbatch, R. J., Krahnmann, G., and Körtzinger, A.: Oxygen variance and
718 meridional oxygen supply in the Tropical North East Atlantic oxygen minimum zone, Climate
719 dynamics, 43, 2999-3024, <https://doi.org/10.1007/s00382-014-2065-0>, 2014.

720 Henson, S. A., Sanders, R., Madsen, E., Morris, P. J., Le Moigne, F., and Quartly, G. D.: A
721 reduced estimate of the strength of the ocean's biological carbon pump, Geophysical Research
722 Letters, 38, 10.1029/2011gl046735, 2011.

723 Kadko, D.: Upwelling and primary production during the US GEOTRACES East Pacific Zonal
724 Transect, Global Biogeochemical Cycles, 31, 218-232, <https://doi.org/10.1002/2016GB005554>,
725 2017.

726 Kaufman, A., Li, Y.-H., and Turekian, K. K.: The removal rates of ^{234}Th and ^{228}Th from waters of
727 the New York Bight, Earth and Planetary Science Letters, 54, 385-392,
728 [https://doi.org/10.1016/0012-821X\(81\)90054-6](https://doi.org/10.1016/0012-821X(81)90054-6), 1981.

729 Keeling, R. F., and Garcia, H. E.: The change in oceanic O_2 inventory associated with recent
730 global warming, Proceedings of the National Academy of Sciences, 99, 7848-7853,
731 10.1073/pnas.122154899, 2002.

732 Kim, G., Hussain, N., and Church, T. M.: How accurate are the ^{234}Th based particulate residence
733 times in the ocean?, *Geophysical research letters*, 26, 619-622,
734 <https://doi.org/10.1029/1999GL900037>, 1999.

735 Ku, T.-L., Knauss, K. G., and Mathieu, G. G.: Uranium in open ocean: concentration and isotopic
736 composition, *Deep Sea Research*, 24, 1005-1017, [https://doi.org/10.1016/0146-6291\(77\)90571-9](https://doi.org/10.1016/0146-6291(77)90571-9),
737 1977.

738 Law, C., Martin, A., Liddicoat, M., Watson, A., Richards, K., and Woodward, E.: A Lagrangian
739 SF6 tracer study of an anticyclonic eddy in the North Atlantic: Patch evolution, vertical mixing
740 and nutrient supply to the mixed layer, *Deep Sea Research Part II: Topical Studies in*
741 *Oceanography*, 48, 705-724, [https://doi.org/10.1016/S0967-0645\(00\)00112-0](https://doi.org/10.1016/S0967-0645(00)00112-0), 2001.

742 Le Moigne, F. A. C., Henson, S. A., Sanders, R. J., and Madsen, E.: Global database of surface
743 ocean particulate organic carbon export fluxes diagnosed from the ^{234}Th technique, *Earth Syst.*
744 *Sci. Data*, 5, 295-304, <https://doi.org/10.5194/essd-5-295-2013>, 2013.

745 Lee, C., Murray, D., Barber, R., Buesseler, K., Dymond, J., Hedges, J., Honjo, S., Manganini, S.,
746 Marra, J., and Moser, C.: Particulate organic carbon fluxes: compilation of results from the 1995
747 US JGOFS Arabian Sea process study: By the Arabian Sea carbon flux group, *Deep Sea*
748 *Research Part II: Topical Studies in Oceanography*, 45, 2489-2501,
749 [https://doi.org/10.1016/S0967-0645\(98\)00079-4](https://doi.org/10.1016/S0967-0645(98)00079-4), 1998.

750 Lüdke, J., Dengler, M., Sommer, S., Clemens, D., Thomsen, S., Krahnemann, G., Dale, A. W.,
751 Achterberg, E. P., and Visbeck, M.: Influence of intraseasonal eastern boundary circulation
752 variability on hydrography and biogeochemistry off Peru, *Ocean Sci. Discuss.*, 2019, 1-31,
753 <https://doi.org/10.5194/os-2019-93>, *in review 2020*.

754 McKee, B. A., DeMaster, D. J., and Nittrouer, C. A.: Uranium geochemistry on the Amazon
755 shelf: Evidence for uranium release from bottom sediments, *Geochimica et Cosmochimica Acta*,
756 51, 2779-2786, [https://doi.org/10.1016/0016-7037\(87\)90157-8](https://doi.org/10.1016/0016-7037(87)90157-8), 1987.

757 Morris, P. J., Sanders, R., Turnewitsch, R., and Thomalla, S.: ^{234}Th -derived particulate organic
758 carbon export from an island-induced phytoplankton bloom in the Southern Ocean, *Deep Sea*
759 *Research Part II: Topical Studies in Oceanography*, 54, 2208-2232,
760 <https://doi.org/10.1016/j.dsr2.2007.06.002>, 2007.

761 Murray, J. W., Downs, J. N., Strom, S., Wei, C.-L., and Jannasch, H. W.: Nutrient assimilation,
762 export production and ^{234}Th scavenging in the eastern equatorial Pacific, *Deep Sea Research Part*
763 *A. Oceanographic Research Papers*, 36, 1471-1489, [https://doi.org/10.1016/0198-0149\(89\)90052-](https://doi.org/10.1016/0198-0149(89)90052-6)
764 [6](https://doi.org/10.1016/0198-0149(89)90052-6), 1989.

765 Nameroff, T., Balistrieri, L., and Murray, J.: Suboxic trace metal geochemistry in the eastern
766 tropical North Pacific, *Geochimica et Cosmochimica Acta*, 66, 1139-1158,
767 [https://doi.org/10.1016/S0016-7037\(01\)00843-2](https://doi.org/10.1016/S0016-7037(01)00843-2), 2002.

768 Noffke, A., Hensen, C., Sommer, S., Scholz, F., Bohlen, L., Mosch, T., Graco, M., and
769 Wallmann, K.: Benthic iron and phosphorus fluxes across the Peruvian oxygen minimum zone,
770 *Limnology and Oceanography*, 57, 851-867, <https://doi.org/10.4319/lo.2012.57.3.0851>, 2012.

771 Osborn, T.: Estimates of the local rate of vertical diffusion from dissipation measurements,
772 *Journal of physical oceanography*, 10, 83-89, [https://doi.org/10.1175/1520-](https://doi.org/10.1175/1520-0485(1980)010<0083:EOTLRO>2.0.CO;2)
773 [0485\(1980\)010<0083:EOTLRO>2.0.CO;2](https://doi.org/10.1175/1520-0485(1980)010<0083:EOTLRO>2.0.CO;2), 1980.

774 Owens, S., Buesseler, K., and Sims, K.: Re-evaluating the ^{238}U -salinity relationship in seawater:
775 Implications for the ^{238}U - ^{234}Th disequilibrium method, *Marine Chemistry*, 127, 31-39,
776 <https://doi.org/10.1016/j.marchem.2011.07.005>, 2011.

777 Owens, S. A., Pike, S., and Buesseler, K. O.: Thorium-234 as a tracer of particle dynamics and
778 upper ocean export in the Atlantic Ocean, Deep Sea Research Part II: Topical Studies in
779 Oceanography, 116, 42-59, <http://dx.doi.org/10.1016/j.dsr2.2014.11.010>, 2015.

780 Peng, Q., Xie, S.-P., Wang, D., Zheng, X.-T., and Zhang, H.: Coupled ocean-atmosphere
781 dynamics of the 2017 extreme coastal El Niño, Nature Communications, 10, 298,
782 10.1038/s41467-018-08258-8, 2019.

783 Pike, S., Buesseler, K., Andrews, J., and Savoye, N.: Quantification of ^{234}Th recovery in small
784 volume sea water samples by inductively coupled plasma-mass spectrometry, Journal of
785 Radioanalytical and Nuclear Chemistry, 263, 355-360, [https://doi.org/10.1007/s10967-005-0594-](https://doi.org/10.1007/s10967-005-0594-z)
786 [z](https://doi.org/10.1007/s10967-005-0594-z), 2005.

787 Puigcorbé, V., Masqué, P., and Le Moigne, F. A. C.: Global database of ratios of particulate
788 organic carbon to thorium-234 in the ocean: improving estimates of the biological carbon pump,
789 Earth Syst. Sci. Data, 12, 1267-1285, 10.5194/essd-12-1267-2020, 2020.

790 Rapp, I., Schlosser, C., Menzel Barraqueta, J. L., Wenzel, B., Lüdke, J., Scholten, J., Gasser, B.,
791 Reichert, P., Gledhill, M., Dengler, M., and Achterberg, E. P.: Controls on redox-sensitive trace
792 metals in the Mauritanian oxygen minimum zone, Biogeosciences, 16, 4157-4182, 10.5194/bg-
793 16-4157-2019, 2019.

794 Rengarajan, R., Sarin, M., and Krishnaswami, S.: Uranium in the Arabian Sea: role of
795 denitrification in controlling its distribution, Oceanologica acta, 26, 687-693,
796 <https://doi.org/10.1016/j.oceact.2003.05.001>, 2003.

797 Resplandy, L., Martin, A. P., Le Moigne, F., Martin, P., Aquilina, A., Mémery, L., Lévy, M., and
798 Sanders, R.: How does dynamical spatial variability impact ^{234}Th -derived estimates of organic
799 export?, Deep Sea Research Part I: Oceanographic Research Papers, 68, 24-45,
800 <https://doi.org/10.1016/j.dsr.2012.05.015>, 2012.

801 Rosengard, S. Z., Lam, P. J., Balch, W. M., Auro, M. E., Pike, S., Drapeau, D., and Bowler, B.:
802 Carbon export and transfer to depth across the Southern Ocean Great Calcite Belt,
803 doi:10.5194/bg-12-3953-2015, 2015.

804 Santschi, P., Murray, J. W., Baskaran, M., Benitez-Nelson, C. R., Guo, L., Hung, C.-C.,
805 Lamborg, C., Moran, S., Passow, U., and Roy-Barman, M.: Thorium speciation in seawater,
806 Marine Chemistry, 100, 250-268, 2006.

807 Savoye, N., Benitez-Nelson, C., Burd, A. B., Cochran, J. K., Charette, M., Buesseler, K. O.,
808 Jackson, G. A., Roy-Barman, M., Schmidt, S., and Elskens, M.: ^{234}Th sorption and export models
809 in the water column: a review, Marine Chemistry, 100, 234-249,
810 <https://doi.org/10.1016/j.marchem.2005.10.014>, 2006.

811 Schafstall, J., Dengler, M., Brandt, P., and Bange, H.: Tidal - induced mixing and diapycnal
812 nutrient fluxes in the Mauritanian upwelling region, Journal of Geophysical Research: Oceans,
813 115, <https://doi.org/10.1029/2009jc005940>, 2010, 2010.

814 Schmidt, S., and Reys, J.: Uranium concentrations of Mediterranean seawater with high
815 salinities, Comptes Rendus de l'Academie des Sciences. Serie 2, 312, 479-484, 1991.

816 Schmidtko, S., Stramma, L., and Visbeck, M.: Decline in global oceanic oxygen content during
817 the past five decades, Nature, 542, 335, 10.1038/nature21399, 2017.

818 Scholz, F., Hensen, C., Noffke, A., Rohde, A., Liebetrau, V., and Wallmann, K.: Early diagenesis
819 of redox-sensitive trace metals in the Peru upwelling area—response to ENSO-related oxygen
820 fluctuations in the water column, Geochimica et Cosmochimica Acta, 75, 7257-7276,
821 10.1016/j.gca.2011.08.007, 2011.

822 Scholz, F., McManus, J., Mix, A. C., Hensen, C., and Schneider, R. R.: The impact of ocean
823 deoxygenation on iron release from continental margin sediments, Nature Geosci, 7, 433-437,
824 <https://doi.org/10.1038/ngeo2162>, 2014.

825 Shepherd, J. G., Brewer, P. G., Oschlies, A., and Watson, A. J.: Ocean ventilation and
826 deoxygenation in a warming world: introduction and overview, Philosophical Transactions of the
827 Royal Society A: Mathematical, Physical and Engineering Sciences, 375, 20170240,
828 doi:10.1098/rsta.2017.0240, 2017.

829 Smith, S. D.: Coefficients for sea surface wind stress, heat flux, and wind profiles as a function of
830 wind speed and temperature, Journal of Geophysical Research: Oceans, 93, 15467-15472,
831 <https://doi.org/10.1029/JC093iC12p15467>, 1988.

832 Steinfeldt, R., Sültenfuß, J., Dengler, M., Fischer, T., and Rhein, M.: Coastal upwelling off Peru
833 and Mauritania inferred from helium isotope disequilibrium, Biogeosciences, 12, 7519-7533,
834 <https://doi.org/10.5194/bg-12-7519-2015>, 2015.

835 Stramma, L., Johnson, G. C., Sprintall, J., and Mohrholz, V.: Expanding oxygen-minimum zones
836 in the tropical oceans, science, 320, 655-658, 2008.

837 Suess, E., Kulm, L., and Killingley, J.: Coastal upwelling and a history of organic-rich mudstone
838 deposition off Peru, Geological Society, London, Special Publications, 26, 181-197, 1987.

839 Swarzenski, P., Campbell, P., Porcelli, D., and McKee, B.: The estuarine chemistry and isotope
840 systematics of $^{234,238}\text{U}$ in the Amazon and Fly Rivers, Continental Shelf Research, 24, 2357-2372,
841 <https://doi.org/10.1016/j.csr.2004.07.025>, 2004.

842 Thomsen, S., Kanzow, T., Krahnemann, G., Greatbatch, R. J., Dengler, M., and Lavik, G.: The
843 formation of a subsurface anticyclonic eddy in the Peru - Chile Undercurrent and its impact on
844 the near - coastal salinity, oxygen, and nutrient distributions, Journal of Geophysical Research:
845 Oceans, 121, 476-501, <https://doi.org/10.1002/2015JC010878>, 2016.

846 Van Der Loeff, M. R., Sarin, M. M., Baskaran, M., Benitez-Nelson, C., Buesseler, K. O.,
847 Charette, M., Dai, M., Gustafsson, Ö., Masque, P., and Morris, P. J.: A review of present

848 techniques and methodological advances in analyzing ^{234}Th in aquatic systems, Marine
849 Chemistry, 100, 190-212, <https://doi.org/10.1016/j.marchem.2005.10.012>, 2006.

850 Waples, J. T., Benitez-Nelson, C., Savoye, N., van der Loeff, M. R., Baskaran, M., and
851 Gustafsson, Ö.: An introduction to the application and future use of ^{234}Th in aquatic systems,
852 Marine Chemistry, 100, 166-189, <https://doi.org/10.1016/j.marchem.2005.10.011>, 2006.

853 Weinstein, S. E., and Moran, S. B.: Vertical flux of particulate Al, Fe, Pb, and Ba from the upper
854 ocean estimated from $^{234}\text{Th}/^{238}\text{U}$ disequilibria, Deep Sea Research Part I: Oceanographic
855 Research Papers, 52, 1477-1488, <https://doi.org/10.1016/j.dsr.2005.03.008>, 2005.

856 Zhurbas, V., and Oh, I. S.: Drifter - derived maps of lateral diffusivity in the Pacific and Atlantic
857 oceans in relation to surface circulation patterns, Journal of Geophysical Research: Oceans, 109,
858 <https://doi.org/10.1029/2003JC002241>, 2004.

859 Zimmerman, J. T. F.: Mixing and flushing of tidal embayments in the western Dutch Wadden Sea
860 part I: Distribution of salinity and calculation of mixing time scales, Netherlands Journal of Sea
861 Research, 10, 149-191, 1976.

862

863

864 Figure captions

865 Figure 1. Maps showing (a) locations of each station from M136 (white squares) and M138 (grey
866 circles) and (B) monthly-averaged current field in the top 15 m from April 16 to May 15, 2017
867 derived from altimetry measurements (<http://marine.copernicus.eu/>; product ID:
868 MULTIOBS_GLO-PHY_REP_015_004). Color boxes in (a) schematically divide the four shelf-
869 offshore transects. Map (a) was created with Ocean Data View (Schlitzer, 2014). The white box
870 in (b) highlights our study area.

871

872 Figure 2. Profiles of ^{238}U (black) and ^{234}Th (orange squares – M136; orange circles – M138)
873 along with concentrations of oxygen (grey) and fluorescence (green). Profiles are organized by
874 cruises, transects, and distance to shore from left to right and top to bottom, indicated by east (E)
875 to west (W) arrows. Error bars for both ^{238}U and ^{234}Th are indicated. Red dashed lines indicate the
876 depth of the mixed layer. The start of the oxygen deficient zone is where oxygen diminishes.
877 Bottom depths are indicated for stations whose bottom depths are shallower than 600 m.

878

879 Figure 3. Shelf-offshore distributions of $^{234}\text{Th}/^{238}\text{U}$ along the four studied transects, as shown in
880 Figure 1, for M136 (left) and M138 (right). White dots denote station location.

881

882 Figure 4. Distributions of averaged ^{234}Th activities during M136 (a, top 30 m) and M138 (b, top
883 50 m).

884

885 Figure 5. Profiles of temperature (solid lines) and salinity (dashed lines) for (a) repeated stations
886 458 (purple) and 508 (yellow), and (d) 495 (blue) and 516 (orange); (b) and (c) respectively
887 profiles for stations 458 and 508 of ^{238}U (black), ^{234}Th (color squares), and concentrations of
888 oxygen (grey) and fluorescence (green). (e) and (f) respectively profiles for stations 495 and 516
889 of ^{238}U (black), ^{234}Th (color squares), and concentrations of oxygen (grey) and fluorescence
890 (green).

891

892 Figure 6. Bar charts of ^{234}Th fluxes due to production and decay (blue), upwelling (orange), and
893 vertical diffusion (grey) for the depths at 5 – 20 m below the ML (top) and 100 m (bottom). Color
894 boxes corresponds to individual transects in Figure 1. Within each transect stations from west
895 (offshore) to east (nearshore) are listed from left to right. Error bars (1SE) are indicated.

896

897 Figure 7. Cross plots of measured ^{238}U activities vs. salinity for M136 (a) and M138 (b), showing
898 poor linear relationship between ^{238}U and salinity. (c) shows a direct comparison between
899 measured and salinity-based ^{238}U to further highlight the large difference between the two. The
900 solid blue line indicates the 1:1 ratio between measured and projected ^{238}U . Blue dashed lines
901 indicate the \pm errors reported in Owens et al. (2011).

Table 1. ²³⁴Th fluxes due to production and decay, upwelling and vertical diffusion below the mixed layer and at 100 m. Horizontal advective fluxes were not quantified at 100 m. Refer to text for details.

Cruise	Station	Mixed layer			Maximum fluorescence	Equilibrium depth	²³⁴ Th flux at the base of the ML						²³⁴ Th flux at 100 m						
		Cast depth	oxycline depth	depth			Depth	Production and decay	Upwelling	Diffusion	Final flux	1 SD	Production and decay	Upwelling	Diffusion	Final flux	1 SD		
		m	m	m	µg L ⁻¹	m	m	dpm m ⁻² d ⁻¹	dpm m ⁻² d ⁻¹	dpm m ⁻² d ⁻¹	dpm m ⁻² d ⁻¹	dpm m ⁻² d ⁻¹	dpm m ⁻² d ⁻¹	dpm m ⁻² d ⁻¹	dpm m ⁻² d ⁻¹	dpm m ⁻² d ⁻¹	dpm m ⁻² d ⁻¹	dpm m ⁻² d ⁻¹	dpm m ⁻² d ⁻¹
M136	353	1	25	102	1.20	100	30	907	52	-36	923	69	1422	-14	2	1410	189		
M136	380	1	26	129	0.87	80	30	1145	0	-41	1105	54	1637	0	-1	1637	132		
M136	402	1	24	129	7.51	100	30	808	0	-75	732	64	1234	0	2	1236	111		
M136	428	1	10	76	4.11	30	30	983	-128	493	1348	129	1772	33	-390	1415	256		
M136	445	1	17	64	2.07	100	30	820	-10	16	826	66	1621	53	6	1681	165		
M136	458	1	5	55	1.61	100	30	1012	-18	161	1155	117	2101	-11	145	2235	238		
M136	472	1	11	29	7.41	200	40	1887	15	-29	1872	77	3315	-12	63	3366	233		
M136	495	1	18	50	1.13	200	30	1149	1	-19	1130	50	3195	2	-5	3192	89		
M136	516	1	16	45	3.77	200	30	614	0	1	615	49	2229	2	-4	2227	109		
M136	547	1	22	48	1.28	150	30	791	0	85	877	61	2510	0	-15	2495	118		
M136	559	1	20	79	1.70	85	50	623	3	-67	559	117	854	-4	2	852	120		
M136	567	1	21	50	2.40	150	30	1593	0	-23	1570	52	3011	0	-11	3000	86		
M138	879	3	43	93	2.24	200	60	1249	0	-16	1266	91	1702	0	-5	1697	111		
M138	882	10	39	211	2.68	150	50	1321	-7	16	1331	63	2264	19	-12	2272	82		
M138	883	12	10	220	1.31	250	30	683	-84	-159	758	108	1782	31	-121	1692	179		
M138	888	7	41	127	1.59	150	50	1364	0	-120	1244	62	1813	0	-4	1809	86		
M138	892	14	47	128	1.05	100	60	1395	33	-118	1309	72	1743	-3	1	1741	99		
M138	898	1	38	101	1.42	60	50	1099	0	-19	1080	104	1091	0	0	1091	125		
M138	904	16	12	72	3.63	150	20	812	275	0	1087	76	2643	0	-9	2634	79		
M138	906	18	32	81	1.73	200	40	1796	0	4	1799	41	3100	0	-1	3100	77		
M138	907	11	31	100	1.29	60	60	1594	-88	13	1518	147	1787	67	-2	1853	140		
M138	912	3	37	70	2.75	>600	50	1960	0	-79	1881	43	2975	0	-3	2972	78		
M138	915	1	26	99	3.51	200	40	1628	0	22	1650	38	2752	0	0	2752	93		
M138	919	1	19	79	4.46	150	30	1316	0	49	1365	32	3249	0	-8	3241	85		

Table 2. Comparison of ^{234}Th fluxes at 100 m calculated with measured ^{238}U activities and those with salinity-based ^{238}U .

Cruise	Station	Cast	^{234}Th fluxes at 100 m*		Difference %
			measured $\text{dpm m}^{-2} \text{d}^{-1}$	predicted $\text{dpm m}^{-2} \text{d}^{-1}$	
M136	353	1	1422	1320	8
M136	380	1	1637	1304	26
M136	402	1	1234	865	43
M136	428	1	1772	1443	23
M136	445	1	1621	1365	19
M136	458	1	2101	1859	13
M136	472	1	3315	3073	8
M136	495	1	3195	3058	4
M136	516	1	2229	2140	4
M136	547	1	2510	2313	9
M136	559	1	854	751	14
M136	567	1	3011	2879	5
M138	879	3	1702	1515	12
M138	882	10	2264	1875	21
M138	883	12	1782	1352	32
M138	888	7	1813	1441	26
M138	892	14	1743	1257	39
M138	898	1	1091	770	42
M138	904	16	2643	2280	16
M138	906	18	3100	2673	16
M138	907	11	1787	1308	37
M138	912	3	2975	2572	16
M138	915	1	2752	2380	16
M138	919	1	3249	2862	14

* For comparison purposes, we only report here ^{234}Th fluxes due to radioactive production and decay.

Table 3. Residence time of total ^{234}Th in the surface layers of Peruvian OMZ.

Cruise	Station	Cast	Average ^{234}Th in	Residence time
			the surface layer* dpm L ⁻¹	days
M136	353	1	1.48	46
M136	380	1	1.35	35
M136	402	1	1.64	61
M136	428	1	1.57	35
M136	445	1	1.64	61
M136	458	1	1.45	38
M136	472	1	0.93	20
M136	495	1	1.20	31
M136	516	1	1.74	85
M136	547	1	1.67	63
M136	559	1	1.75	94
M136	567	1	1.41	45
M138	879	3	1.59	75
M138	882	10	1.81	69
M138	883	12	1.87	74
M138	888	7	1.68	67
M138	892	14	1.69	65
M138	898	1	1.66	92
M138	904	16	1.32	24
M138	906	18	1.15	25
M138	907	11	1.04	41
M138	912	3	1.25	33
M138	915	1	1.16	28
M138	919	1	1.17	26

* Here 'surface layer' refers to the top 30 m during M136 and top 50 m during M138.

Figure 1

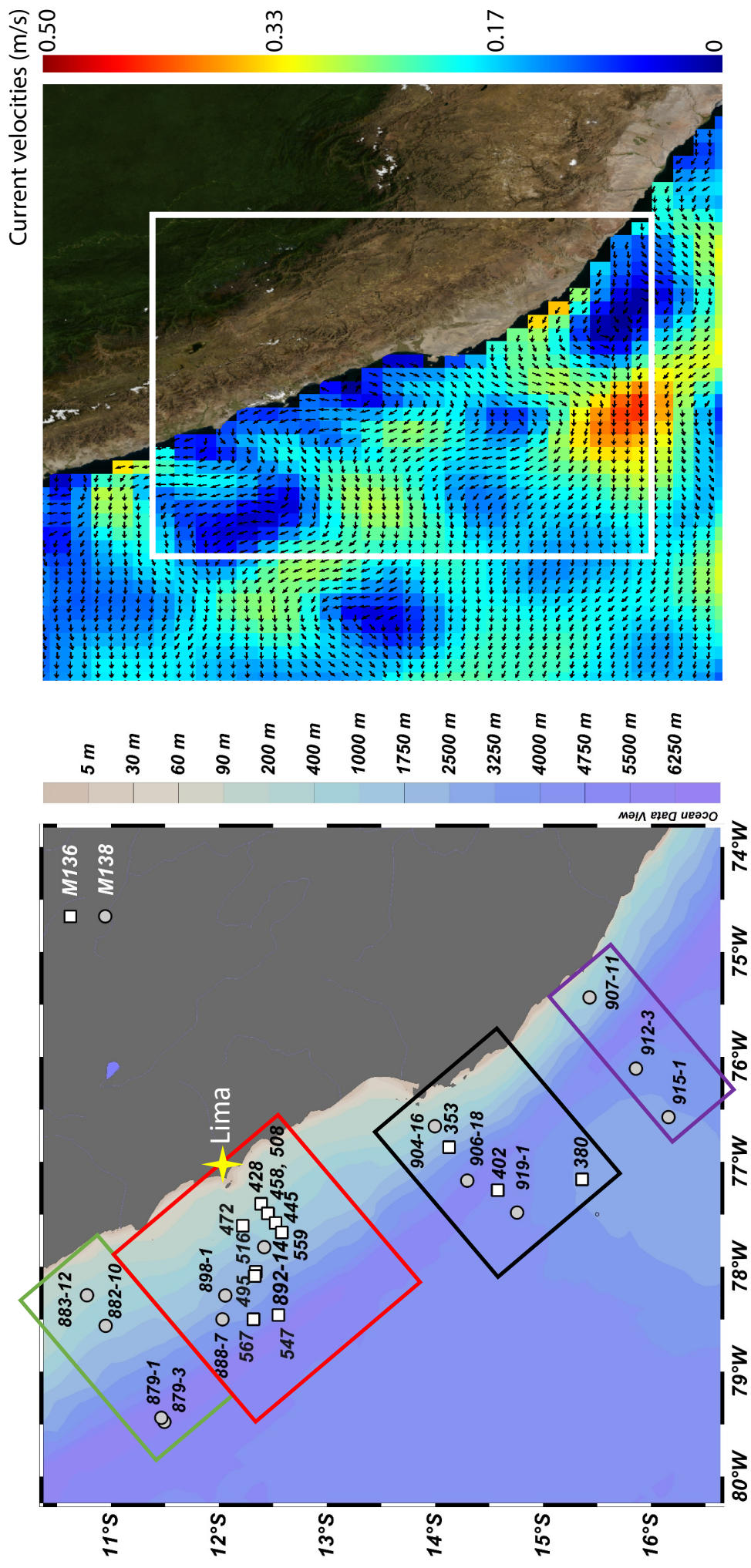
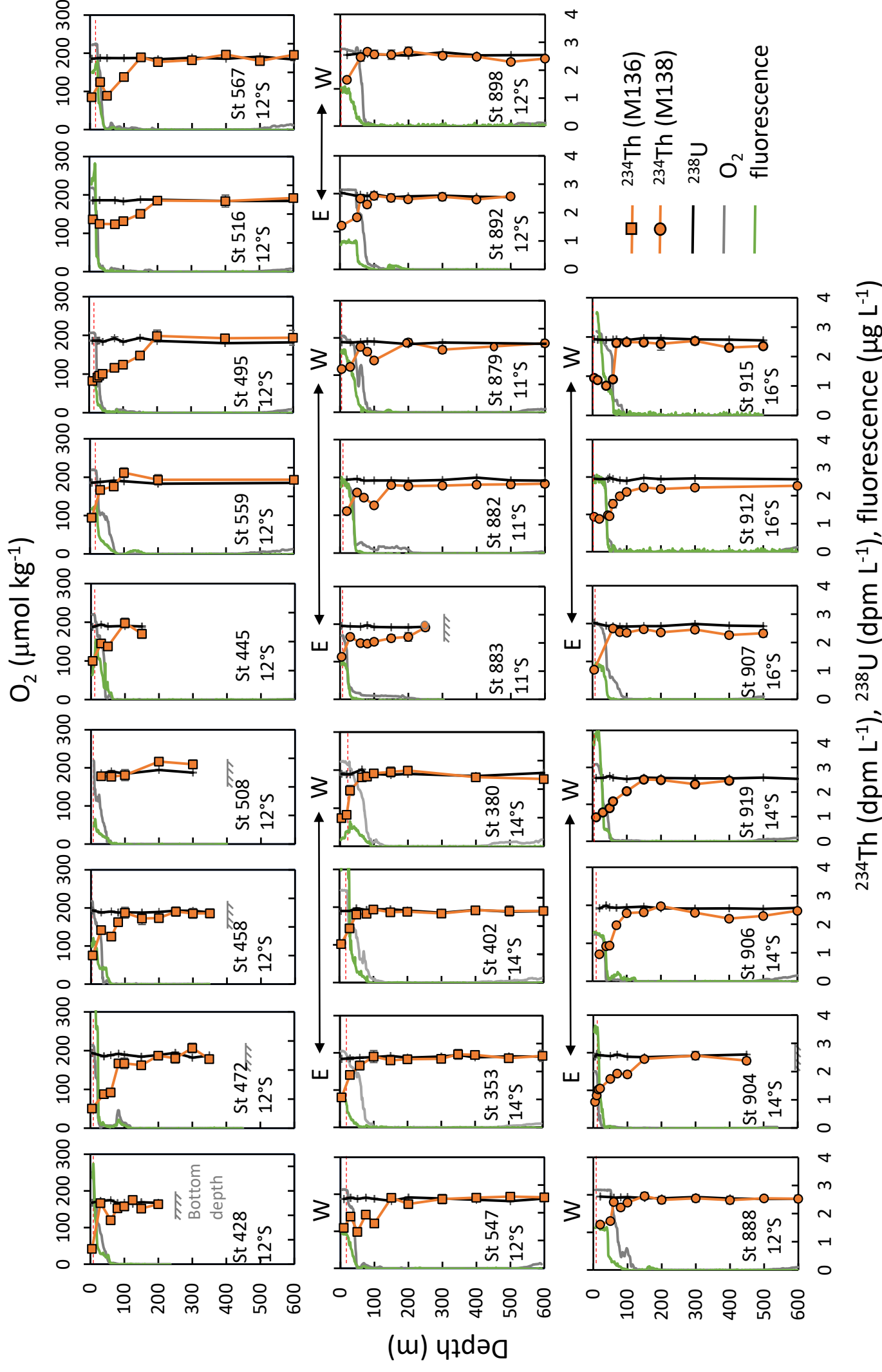


Figure 2

E ← → W



^{234}Th (dpm L^{-1}), ^{238}U (dpm L^{-1}), fluorescence ($\mu\text{g L}^{-1}$)

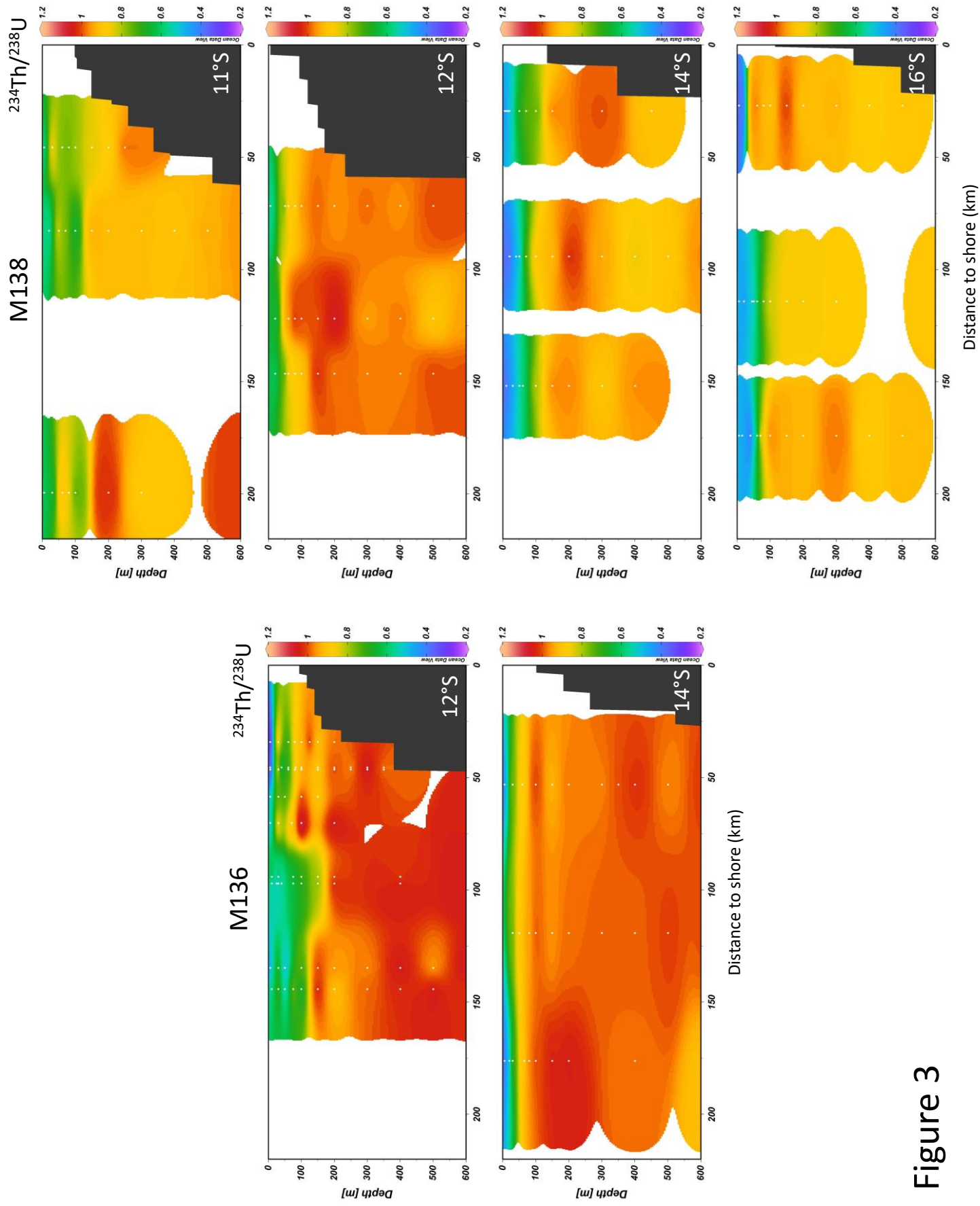


Figure 3

Figure 4

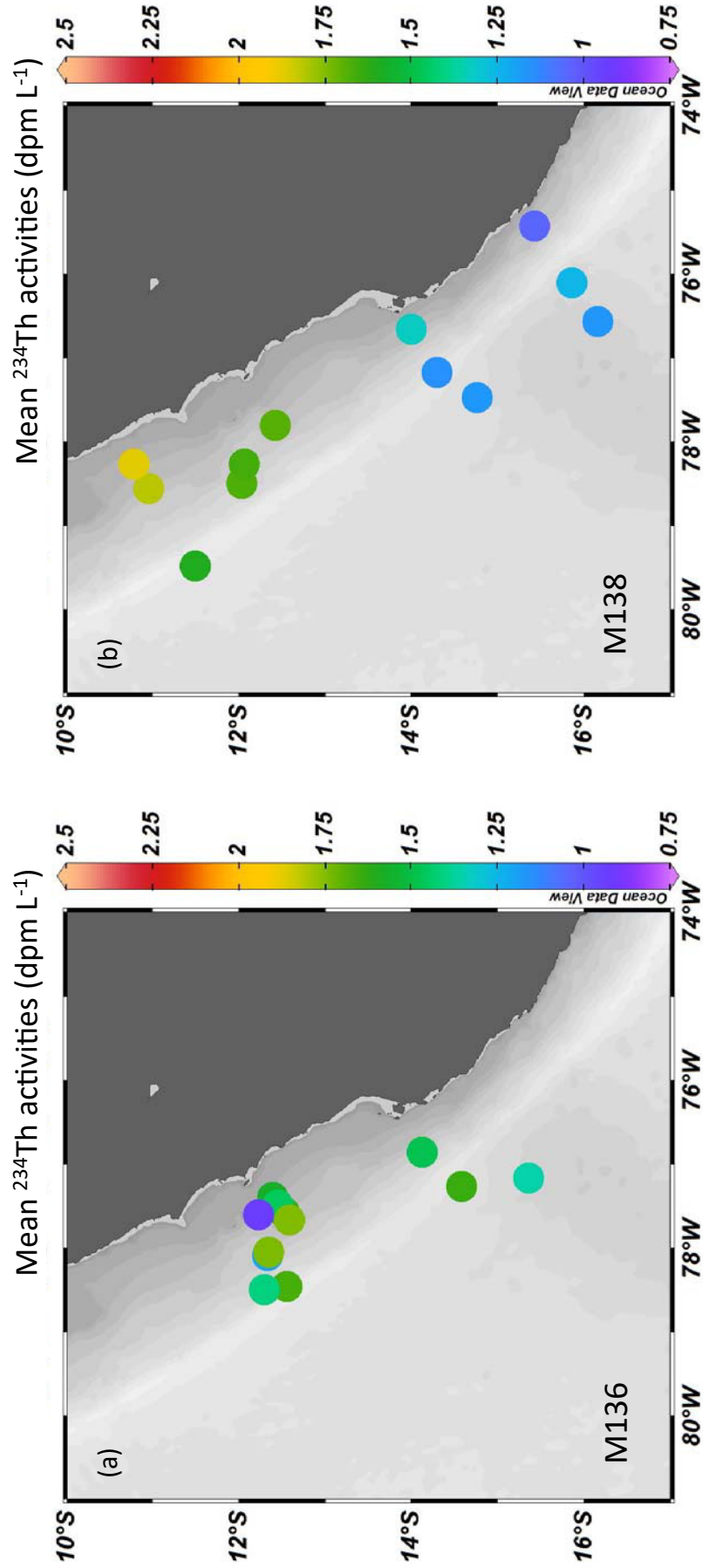


Figure 5

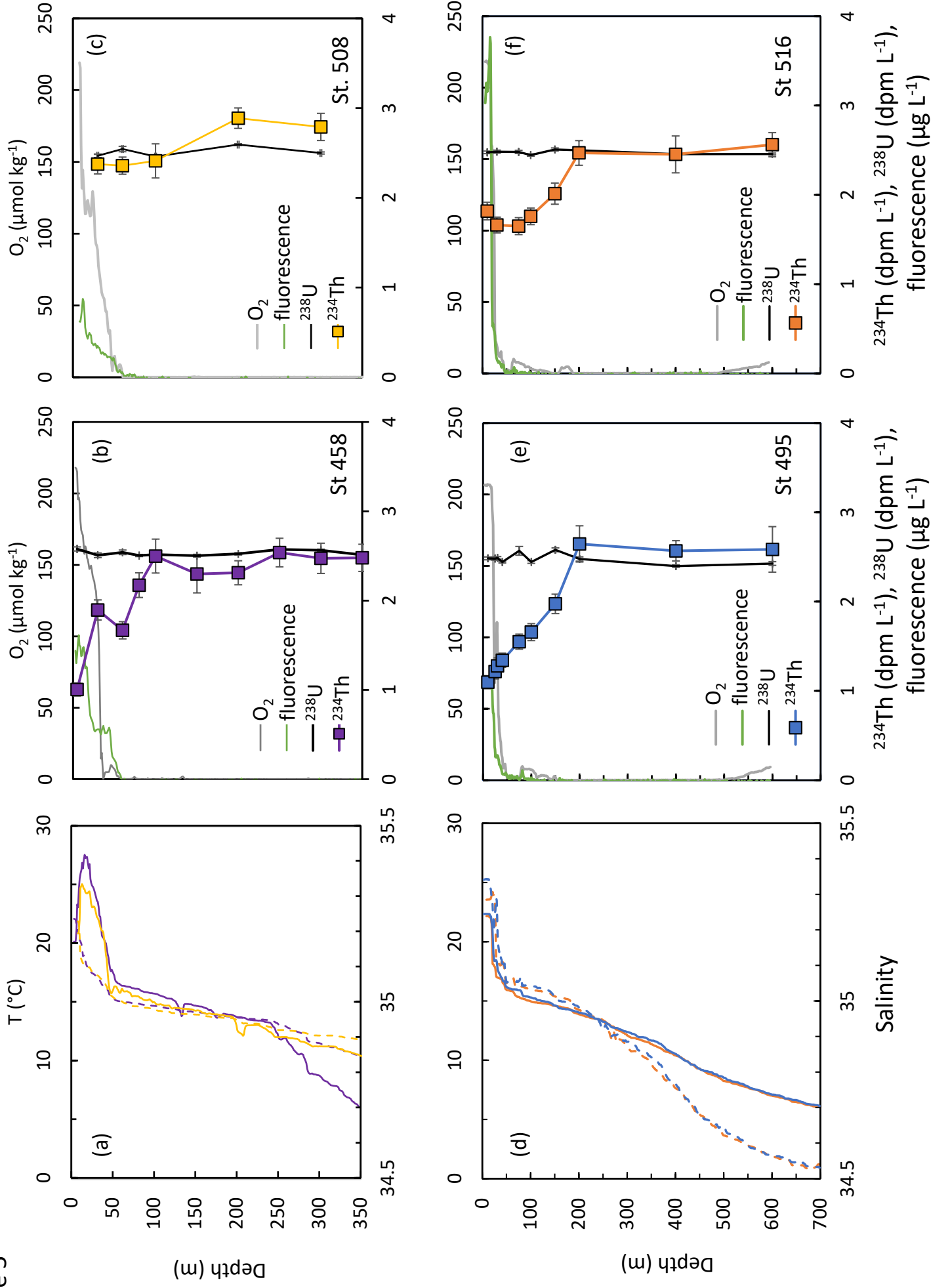


Figure 6

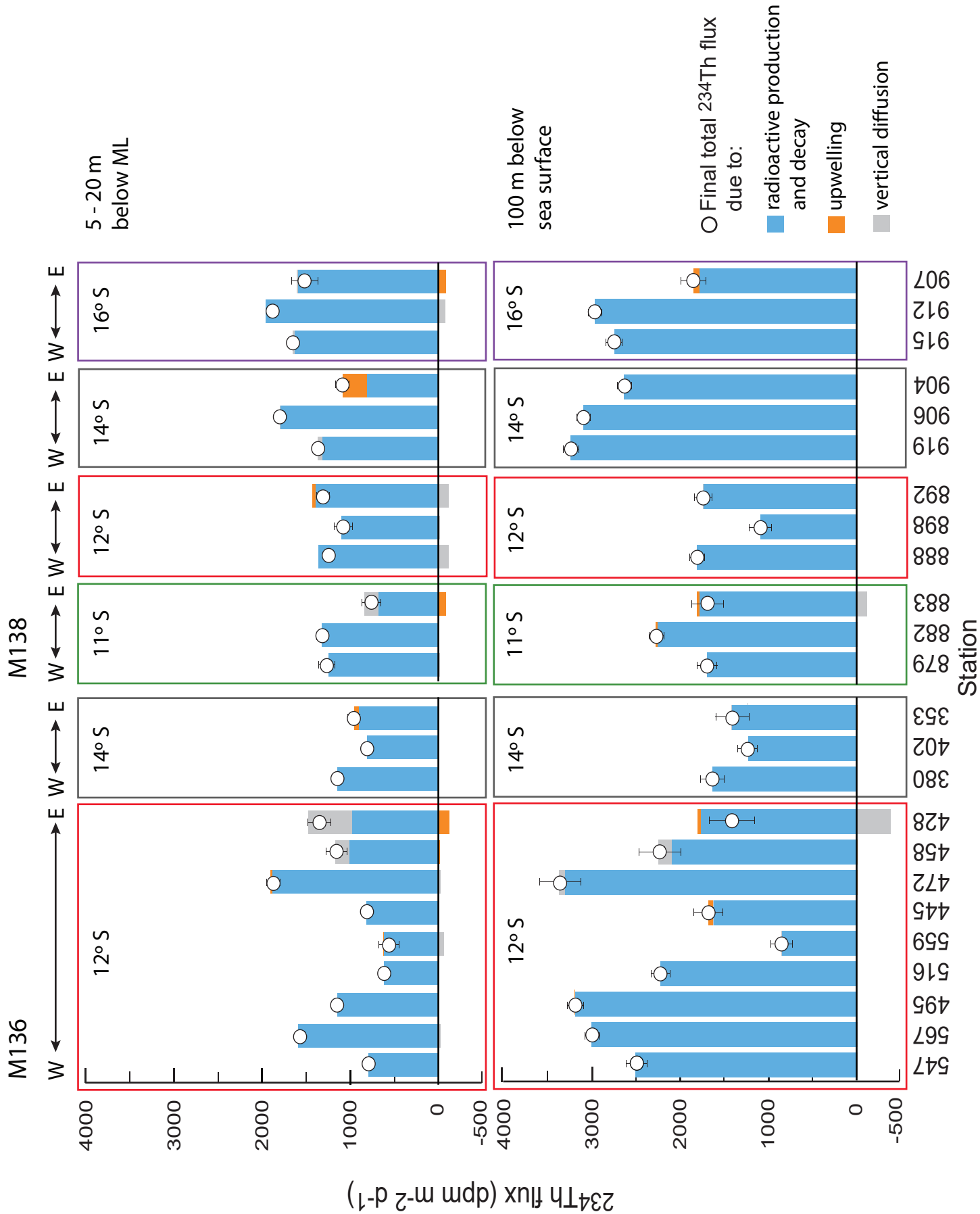


Figure 7

